Eur. Phys. J. A (2013) **49**: 100
DOI 10.1140/epja/i2013-13100-2

THE EUROPEAN PHYSICAL JOURNAL A

Regular Article – Theoretical Physics

Dissecting deuteron Compton scattering I: The observables with polarised initial states

Harald W. Grießhammer[a]

[1] Institut für Kernphysik (IKP-3), Institute for Advanced Simulation and Jülich Centre for Hadron Physics, Forschungszentrum Jülich, D-52428 Jülich, Germany
[2] Institute for Nuclear Studies, Department of Physics, The George Washington University, Washington DC 20052, USA[b]

Received: 24 April 2013
Published online: 6 August 2013 –
Communicated by M.C. Birse

For Karl Heinz Lindenberger (1925–2012)

Abstract. A complete set of linearly independent observables in Compton scattering with arbitrarily polarised real photons off an arbitrarily polarised spin-1 target is introduced, for the case that the final-state polarisations are not measured. Adopted from the one widely used, *e.g.*, in deuteron photo-dissociation, it consists of 18 terms: the unpolarised cross section, the beam asymmetry, 4 target asymmetries and 12 asymmetries in which both beam and target are polarised. They are expressed by the helicity amplitudes and —where available— related to observables discussed by other authors. As application to deuteron Compton scattering, their dependence on the (isoscalar) scalar and spin dipole polarisabilities of the nucleon is explored in Chiral Effective Field Theory with dynamical $\Delta(1232)$ degrees of freedom at order $e^2\delta^3$. Some asymmetries are sensitive to only one or two dipole polarisabilities, making them particularly attractive for experimental studies. At a photon energy of 100 MeV, a set of 5 observables is identified from which one may be able to extract the spin polarisabilities of the nucleon. These are experimentally realistic but challenging and mostly involve tensor-polarised deuterons. Relative to Compton scattering from a nucleon, sensitivity to the "mixed" spin polarisabilities γ_{E1M2} and γ_{M1E2} is increased because of the interference with the D wave component of the deuteron and with its pion-exchange current. An interactive *Mathematica 9.0* notebook with results for all observables at photon energies up to 120 MeV is available from `hgrie@gwu.edu`.

1 Introduction

Compton scattering $\gamma\mathrm{X} \to \gamma\mathrm{X}$ at energies below 1 GeV explores the two-photon response of the internal low-energy degrees of freedom in the nucleon and in the lightest nuclei. Since the electric and magnetic fields of a real photon induce radiation multipoles by displacing the charged constituents and currents in the target, energy-dependence and multipolarity of the emitted radiation test the symmetries and strengths of the interactions between and with them; see a recent review for details [1]. In deuteron Compton scattering, one has access not only to the proton and neutron response, but also to how photons couple to the charged pion-exchange currents, thus testing nuclear binding in the simplest stable few-nucleon system. In addition, the constructive interference with the D wave component of the deuteron can be expected to lead to increased sensitivity of the hadronic response to the quadrupole components of the photon fields.

A new generation of high-luminosity facilities like HIγS, MAMI and MAX-Lab with near-100% linear or circular beam polarisation have started to explore these opportunities. Dense deuteron targets with vector polarisations approaching 90% are standard. Since tensor and vector polarisations are related when in thermal equilibrium with a solid lattice, most vector-polarised deuteron targets automatically also provide tensor polarisation degrees of $\lesssim 75\%$ —and the potential for greater values in dedicated set-ups [2–4].

Now is thus an opportune moment for a comprehensive classification of independent deuteron amplitudes and observables. The spin-$\frac{1}{2}$ case has been discussed by Babusci *et al.* [5]. For the deuteron, Chen, Ji and Li [6] constructed a basis for those 12 amplitudes which remain linearly independent after parity and time-reversal invariance have been invoked on the [2(photon helicities) × 3(deuteron helicities)]^2 (both in- and out-state) = 36 helicity amplitudes. However, a corresponding list of 23 independent observables (12 complex amplitudes minus an overall phase) is missing. While several single- and double-

[a] e-mail: `hgrie@gwu.edu`
[b] Permanent address.

polarisation observables have been constructed and their sensitivity to the nucleon polarisabilities explored [6–10], no systematic study of vector and tensor polarisation observables exists. Only one tensor observable has been considered explicitly, namely for an unpolarised beam [11–13]. What is more, some deuteron "vector" observables which were defined analogous to the spin-$\frac{1}{2}$ case will be shown to actually receive contributions from both vector and tensor polarisations.

For the case that the polarisations of the final state are not detected, this work aims to classify all 18 independent observables and their relation to the helicity amplitudes. At present, this seems to be the experimentally most feasible situation. Instead of simply extending the work by Babusci *et al.* to the spin-1 case, the starting point is the most general cross section of an arbitrarily polarised photon beam on an arbitrarily polarised spin-1 target, in a form which is well known, *e.g.*, from deuteron photo-disintegration [14]. It is parametrised in terms of the unpolarised cross section, 1 beam and 4 target asymmetries as well as 12 double asymmetries, and has the added benefit that experiments in less-than-ideal settings can easily be described as well, like when residual or mixed target and beam polarisations exist. A future publication will define and study 5 additional independent polarisation transfer observables [15]. A complete set of independent Compton scattering observables will then be available from which the 23 real parameters which characterise deuteron Compton scattering (*i.e.* its independent amplitudes) can be reconstructed in full.

The second part of this article explores the sensitivity of the 18 observables to the two-photon response of the individual nucleon. Remember that the proportionality constants between the electric or magnetic field of the incident photon and the radiation multipoles induced in each nucleon are the energy-dependent (dynamical) polarisabilities of the nucleon [16,17]. They parametrise the stiffness of the nucleon N (spin $\frac{\vec{\sigma}}{2}$) against transitions $Xl \to Yl'$ of definite photon multipolarity at frequency ω ($l' = l \pm \{0;1\}$; $X,Y = E,M$; $T_{ij} = \frac{1}{2}(\partial_i T_j + \partial_j T_i)$; $T = E,B$); see, *e.g.*, [1,18] and references therein. Rewritten as point-like interactions between photons and nucleons, the terms which contain photon dipoles read

$$\begin{aligned} &2\pi\, N^\dagger \Big[\alpha_{E1}(\omega)\vec{E}^2 + \beta_{M1}(\omega)\vec{B}^2 + \gamma_{E1E1}(\omega)\vec{\sigma}\cdot(\vec{E}\times\dot{\vec{E}}\,) \\ &+\gamma_{M1M1}(\omega)\,\vec{\sigma}\cdot(\vec{B}\times\dot{\vec{B}}\,) - 2\gamma_{M1E2}(\omega)\,\sigma^i\,B^j\,E_{ij} \\ &+2\gamma_{E1M2}(\omega)\,\sigma^i\,E^j\,B_{ij} + \ldots\Big]\, N. \end{aligned} \tag{1}$$

Since each interaction with a photon leaves a unique signal in such dispersive effects, Compton scattering allows one to study the symmetries and dynamics of the hadronic constituents in detail.

The zero-energy values, $\alpha_{E1} := \alpha_{E1}(\omega = 0)$ etc., are often quoted as "the (static) polarisabilities". Two scalar polarisabilities $\alpha_{E1}(\omega)$ and $\beta_{M1}(\omega)$ parametrise electric and magnetic dipole transitions. The four dipole spin polarisabilities $\gamma_{E1E1}(\omega)$, $\gamma_{M1M1}(\omega)$, $\gamma_{E1M2}(\omega)$ and $\gamma_{M1E2}(\omega)$ encode the response of the nucleon spin-structure. These are particularly interesting since, intuitively interpreted, they parametrise the bi-refringence which the electromagnetic field associated with the spin degrees causes in the nucleon, in analogy to the classical Faraday-effect [18]. The information accessible in Compton scattering thus goes well beyond that in tests of the one-photon response, *e.g.*, in form factor experiments.

Theoretical input is of course needed to carefully evaluate data consistency in one model-independent framework for hidden systematic errors; to identify the underlying mechanisms using minimal theoretical bias, like the detailed chiral dynamics of the pion cloud and of the $\Delta(1232)$ as the lowest nucleon resonance; and, most importantly, to explain how these findings emerge from QCD by relating to emerging lattice simulations (see the most recent papers [19–21]). The polarisabilities also enter as one of the biggest sources of uncertainties in theoretical determinations of the proton-neutron mass shift (see, *e.g.*, the most recently published [22]) and of the two-photon-exchange contribution to the Lamb shift in muonic hydrogen [23–25]. While presumably not providing a solution to the proton-charge-radius puzzle, they also contribute in radiative corrections to this process, see, *e.g.*, [26]. For all these goals, Chiral Effective Field Theory (χEFT), the low-energy theory of QCD and extension of Chiral Perturbation Theory to few-nucleon systems, adds objective estimates of the theoretical uncertainties. Indeed, χEFT has been particularly successful in describing proton and few-nucleon Compton scattering, starting with the first calculation and sensitivity study of the scalar polarisabilities in χEFT [27,28]. Reference [1] contains details on its history and status in Compton scattering, as well as on χEFT variants not discussed here.

Having established a consistent database from all available proton and deuteron data below 350 MeV in ref. [1], the static scalar polarisabilities of the proton were recently extracted in this framework with a χ^2 per degree of freedom of 113/135 [29]:

$$\begin{aligned} \alpha_{E1}^{(\mathrm{p})} &= 10.7 \pm 0.3(\mathrm{stat}) \pm 0.2(\mathrm{Baldin}) \pm 0.3(\mathrm{theory}) \\ \beta_{M1}^{(\mathrm{p})} &= 3.1 \mp 0.3(\mathrm{stat}) \pm 0.2(\mathrm{Baldin}) \mp 0.3(\mathrm{theory}). \end{aligned} \tag{2}$$

Throughout, polarisabilities without superscripts denote isoscalar quantities, and the canonical units of $10^{-4}\,\mathrm{fm}^3$ for scalar and $10^{-4}\,\mathrm{fm}^4$ for spin dipole polarisabilities are understood.

Since the deuteron is isoscalar, the elastic scattering on it provides of course only access to the isoscalar (average) nucleon polarisabilities. In ref. [1], these were found to have much larger errors since deuteron data is less accurate and more scarce (with $\chi^2/\mathrm{d.o.f.} = 24/25$):

$$\begin{aligned} \alpha_{E1} &= 10.9 \pm 0.9(\mathrm{stat}) \pm 0.2(\mathrm{Baldin}) \pm 0.8(\mathrm{theory}) \\ \beta_{M1} &= 3.6 \mp 0.9(\mathrm{stat}) \pm 0.2(\mathrm{Baldin}) \mp 0.8(\mathrm{theory}). \end{aligned} \tag{3}$$

These results were derived using the Baldin sum rules, whose isoscalar variant reads [1]

$$\alpha_{E1} + \beta_{M1} = 14.5 \pm 0.3. \tag{4}$$

These publications also discuss in detail the fit procedure and residual theoretical uncertainties. Comparing eqs. (2) and (3) shows that within the data-dominated error, the two-photon responses of the proton and neutron as parametrised by the scalar polarisabilities are identical. A particularly interesting prediction of χEFT is that small proton-neutron differences stem from chiral–symmetry-breaking interactions with and in the pion cloud around the nucleon, probing details of QCD. Experiments are therefore underway and planned to improve the Compton scattering database; see, *e.g.*, [1] for details. Their other focus are the spin polarisabilities. Only the linear combinations γ_0 and γ_π of scattering under 0° and 180° are somewhat constrained by data or phenomenology. Conflicting results from MAMI and LEGS exist for the proton, and large error bars are found for the neutron [30]. The isoscalar values are in the range (see also [10])

$$\begin{aligned}\gamma_0 &:= -\gamma_{E1E1} - \gamma_{M1M1} - \gamma_{E1M2} - \gamma_{M1E2} \approx 0,\\ \gamma_\pi &:= -\gamma_{E1E1} + \gamma_{M1M1} - \gamma_{E1M2} + \gamma_{M1E2}\\ &\approx [5\ldots15].\end{aligned} \tag{5}$$

A comprehensive classification of independent amplitudes and observables is thus warranted, including a detailed study of dependencies on scalar and spin polarisabilities. Insofar, this publication extends the so-far most thorough work in ref. [10], including its erratum.

After defining the most general cross section without detection of the polarisations of the final state in subsect. 2.2, the remainder of sect. 2 is devoted to the more technical issues of relating its observables to the helicity amplitudes of deuteron Compton scattering and to other parameter combinations found in the literature, including the Babusci classification. Section 3 discusses the sensitivity of the observables to the dipole polarisabilities, with an eye towards potential experiments. It also proposes a road-map to the isoscalar, spin-independent and spin-dependent nucleon polarisabilities from high-accuracy experiments with deuteron targets. A customary summary in sect. 4 rounds off the article. Preliminary results were presented in a recent proceeding [31].

2 Constructing observables

2.1 Kinematics and polarisation states

This presentation follows the reviews of Arenhövel and Sanzone [14], and Paetz [2]. Inspired by the former, the kinematics is pictorially represented in fig. 1. The photon beam polarisation is described by a density matrix with entries

$$\begin{aligned}(\rho^{(\gamma)})_{\lambda\lambda'} &:= \langle\lambda'|\rho^{(\gamma)}|\lambda\rangle\\ &= \frac{1}{2}\left[\delta_{\lambda\lambda'}(1+\lambda\,P^{(\gamma)}_{\rm circ}) - \delta_{\lambda,-\lambda'}\,P^{(\gamma)}_{\rm lin}\,e^{-2\lambda{\rm i}\varphi_{\rm lin}}\right].\end{aligned} \tag{6}$$

Here, $P^{(\gamma)}_{\rm circ} \in [-1;1]$ is the degree of right circular polarisation, *i.e.* the difference between right and left circular polarisation, with $P^{(\gamma)}_{\rm circ} = +1/-1$ describing a fully right/left circularly polarised photon (positive/negative helicities $\lambda, \lambda' = \pm$ by $\vec{e}_\pm = -\frac{\rm i}{\sqrt{2}}(\vec{e}_y \pm {\rm i}\vec{e}_x)$). The degree of linear polarisation is parametrised by $P^{(\gamma)}_{\rm lin} \in [0;1]$, with $\varphi_{\rm lin} \in [0;\pi[$ the angle from the x-axis to the polarisation plane[1], *i.e.* a photon polarisation $\vec{\epsilon}_{\rm lin} = \vec{e}_x\cos\varphi_{\rm lin} + \vec{e}_y\sin\varphi_{\rm lin}$.

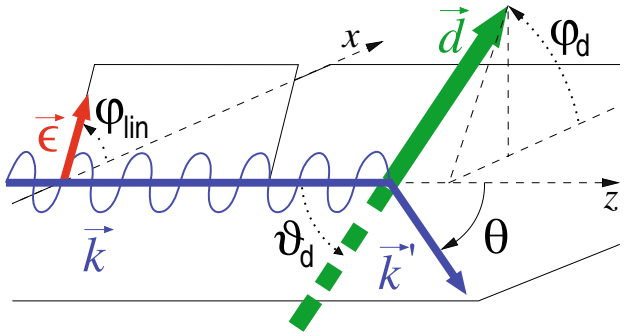

Fig. 1. (Colour on-line) Kinematics of deuteron Compton scattering: incoming photon along the z-axis, linearly polarised at an angle $\varphi_{\rm lin}$ relative to the scattering plane (xz-plane); scattering angle θ; deuteron polarisation axis $\vec{d}$ with azimuthal angle $\vartheta_{\rm d}$ from the z-axis to $\vec{d}$, and polar angle $\varphi_{\rm d}$ from the x-axis to the projection of $\vec{d}$ onto the xy-plane; y-axis the normal of the scattering plane; $\vec{k}$ ($\vec{k}'$) the momentum of the incident (outgoing) photon.

Today's deuteron targets are both vector- and tensor-polarised along the same axis [2]. Let the axis $\vec{d}$ in which $\rho^{(\rm d)}$ is diagonal be oriented as in fig. 1, *i.e.*[2]

$$\vec{d} = \begin{pmatrix}\sin\vartheta_{\rm d}\,\cos\varphi_{\rm d}\\ \sin\vartheta_{\rm d}\,\sin\varphi_{\rm d}\\ \cos\vartheta_{\rm d}\end{pmatrix}, \tag{7}$$

with azimuthal angle $\vartheta_{\rm d} \in [0;\pi]$ and polar angle $\varphi_{\rm d} \in [0;2\pi]$. The entries of the polarisation density matrix are then in the basis $M_{\vec{d}} = (1;0;-1)$ of magnetic quantum numbers along $\vec{d}$:

$$\begin{aligned}\rho^{(\rm d)}_{\vec{d}} = \frac{1}{3}\Bigg[&P^{(\rm d)}_0\,1 + \sqrt{\frac{3}{2}}\,P^{(\rm d)}_1\begin{pmatrix}1&0&0\\0&0&0\\0&0&-1\end{pmatrix}\\ &+\frac{1}{\sqrt{2}}\,P^{(\rm d)}_2\begin{pmatrix}1&0&0\\0&-2&0\\0&0&1\end{pmatrix}\Bigg].\end{aligned} \tag{8}$$

The subscript denotes of course that the system is quantised along the $\vec{d}$-axis, not the z-axis, and is kept for comparison with the literature [2, 14]. Here, $P^{(\rm d)}_0 := 1$ parametrises the part of the deuteron density matrix which behaves like a scalar under rotations, while $P^{(\rm d)}_1$ and $P^{(\rm d)}_2$ characterise the parts which transform like an (irreducible) spherical vector and tensor operator, respectively.

[1] This definition varies from that of [14], whose angle ϕ is counted *from* the polarisation plane *to* the normal of the scattering plane, *i.e.* $\varphi_{\rm lin} = -\phi$.

[2] This definition varies from that of [14], whose angles are defined as $\phi_{\rm d} - \phi = \varphi_{\rm d}$, but still $\theta_{\rm d} = \vartheta_{\rm d}$.

These can be related to the degrees of vector and tensor polarisation in Cartesian coordinates: along this quantisation axis, a fraction $1 \geq p_{\pm,0} \geq 0$ populates the state with magnetic quantum number $M_{\vec{d}} = \pm 1, 0$. The overall norm is $p_+ + p_- + p_0 = 1$. The degree of vector polarisation is in Cartesian coordinates $P_z = p_+ - p_- = \sqrt{\frac{2}{3}}\, P_1^{(\mathrm{d})} \in [-1;1]$, and that of tensor polarisation is $P_{zz} = p_+ + p_- - 2p_0 = 1 - 3p_0 = \sqrt{2}\, P_2^{(\mathrm{d})} \in [1;-2]$. Because $p_{\pm,0}$ lies between 0 and 1, they are subject to the combined constraint $2\sqrt{2} \geq P_2^{(\mathrm{d})} + \sqrt{3}\,|P_1^{(\mathrm{d})}| \geq -\sqrt{2}$. When the deuteron spins are in thermal equilibrium with a solid lattice, tensor and vector polarisations are related by $P_{zz} = 2 - \sqrt{4 - 3P_z^2}$, *i.e.* $P_2^{(\mathrm{d})} = \sqrt{2} - \sqrt{2 - (P_1^{(\mathrm{d})})^2}$ [2,3].

The advantage to decompose $\rho^{(\mathrm{d})}$ into irreducible representations of the rotation group is that it is then particularly simple to change the quantisation axis from $\vec{d}$ to the beam axis $\hat{\vec{k}} := \vec{k}/\omega \equiv \vec{e}_z$ (cf. [32], subsect. 13). Reference [14] finally provides the angular momentum representation of the spin-1 polarisation density matrix which is diagonal along $\vec{d}$:

$$\rho^{(\mathrm{d})}_{mm'} := \langle m'|\rho^{(\mathrm{d})}|m\rangle = \frac{(-1)^{1-m}}{\sqrt{3}} \sum_{I=0}^{2} \sqrt{2I+1}\, P_I^{(\mathrm{d})} \times \sum_{M=-I}^{I} \begin{pmatrix} 1 & 1 & I \\ m & -m' & -M \end{pmatrix} e^{\mathrm{i}M\varphi_{\mathrm{d}}}\, d^I_{M0}(\vartheta_{\mathrm{d}}). \quad (9)$$

The conventions for $3j$ symbols and reduced Wigner-d matrices are those of Rose [32] and Edmonds [33], also listed in the *Particle Data Booklet* [34].

2.2 Parametrising the cross section

Like any reaction $\gamma\mathrm{d} \to \mathrm{X}$, deuteron Compton scattering and deuteron photo-disintegration share the same in-state. As long as the final-state polarisations are not detected (*i.e.* are summed over), their differential cross sections are thus characterised by the same dependence on the initial-state deuteron and photon polarisations. One can therefore adopt the decomposition familiar from deuteron photo-disintegration [14] to Compton scattering:

$$\begin{aligned} \frac{\mathrm{d}\sigma}{\mathrm{d}\Omega} = \left.\frac{\mathrm{d}\sigma}{\mathrm{d}\Omega}\right|_{\mathrm{unpol}} \Bigg[& 1 + \Sigma^{\mathrm{lin}}(\omega,\theta)\, P_{\mathrm{lin}}^{(\gamma)}\, \cos 2\varphi_{\mathrm{lin}} \\ & + \sum_{\substack{I=1,2 \\ 0\leq M\leq I}} T_{IM}(\omega,\theta)\, P_I^{(\mathrm{d})}\, d^I_{M0}(\vartheta_{\mathrm{d}})\, \cos\left[M\varphi_{\mathrm{d}} - \frac{\pi}{2}\delta_{I1}\right] \\ & + \sum_{\substack{I=1,2 \\ 0\leq M\leq I}} T^{\mathrm{circ}}_{IM}(\omega,\theta) P_I^{(\mathrm{d})}\, d^I_{M0}(\vartheta_{\mathrm{d}}) P_{\mathrm{circ}}^{(\gamma)} \sin\left[M\varphi_{\mathrm{d}} + \frac{\pi}{2}\delta_{I1}\right] \\ & + \sum_{\substack{I=1,2 \\ -I\leq M\leq I}} T^{\mathrm{lin}}_{IM}(\omega,\theta)\, P_I^{(\mathrm{d})}\, d^I_{M0}(\vartheta_{\mathrm{d}}) \\ & \qquad \times P_{\mathrm{lin}}^{(\gamma)}\, \cos\left[M\varphi_{\mathrm{d}} - 2\varphi_{\mathrm{lin}} - \frac{\pi}{2}\delta_{I1}\right] \Bigg]. \end{aligned} \quad (10)$$

Besides the trivial limitations $I \in \{0;1;2\}$ and $|M| \leq I$, the summations in eq. (10) are easily shown to be constrained by trivial zeros and double counting of angular dependencies:

- $T_{00} \equiv 1$, *i.e.* the first factor in eq. (10) could also be written as $1 \equiv T_{00}\, P_0^{(\mathrm{d})}$;
- $T_{IM} = (-)^{I+M}\, T_{I,-M}$, and in particular $T_{10} \equiv 0$;
- $T^{\mathrm{circ}}_{IM} = (-)^{I+M+1}\, T^{\mathrm{circ}}_{I,-M}$, and in particular $T^{\mathrm{circ}}_{00} \equiv 0$ (the circular-beam asymmetry on an unpolarised target, identical zero due to rotation invariance) and $T^{\mathrm{circ}}_{20} \equiv 0$;
- $T^{\mathrm{lin}}_{00} \equiv \Sigma^{\mathrm{lin}}$.

The cross section is thus fully parametrised by the following linearly independent functions:

- 1 differential cross section $\left.\frac{\mathrm{d}\sigma}{\mathrm{d}\Omega}\right|_{\mathrm{unpol}}$ of unpolarised photons on an unpolarised target;
- 1 beam asymmetry of a linearly polarised beam on an unpolarised target Σ^{lin};
- 1 vector target asymmetry of an unpolarised beam T_{11};
- 3 tensor target asymmetries on an unpolarised beam T_{2M}, $M = 0, 1, 2$;
- 2 double asymmetries of circular photons on a vector polarised target T^{circ}_{1M}, $M = 0, 1$;
- 2 double asymmetries of circular photons on a tensor polarised target T^{circ}_{2M}, $M = 1, 2$;
- 3 double asymmetries of linear photons on a vector target T^{lin}_{1M}, $M = 0, \pm 1$;
- 5 double asymmetries of linear photons on a tensor target T^{lin}_{2M}, $M = 0, \pm 1, \pm 2$.

Since these 18 real, independent functions of scattering energy and angle are of course process-dependent, those discussed in Compton scattering differ from those in, *e.g.*, deuteron photo-disintegration. The decomposition of eq. (10) holds in any frame, but the functions are frame-dependent. It also applies when the polarisation of the target and/or scattered photon is detected in the final state, without specifying the initial state. The 18 recoil polarisations are thus identical to the functions above.

2.3 Matching helicity amplitudes to observables

Deuteron Compton scattering amplitudes T are usually described in the helicity basis (dependencies on ω, θ and other parameters are dropped for brevity in this section),

$$A^{M_f\lambda_f}_{M_i\lambda_i} := \langle M_f, \lambda_f | T | M_i, \lambda_i \rangle, \quad (11)$$

where $\lambda_{i/f} = \pm$ is the circular polarisation of the initial/final photon, and $M_{i/f} \in \{0; \pm 1\}$ is the magnetic quantum number of the initial/final deuteron spin. In the following, the indices and summations over the final-state polarisations are suppressed as self-understood, *e.g.*, $A_{M_i\lambda_i} \equiv A^{M_f\lambda_f}_{M_i\lambda_i}$. In addition, it is convenient to introduce an abbreviation for the sum over all polarisations of the squared amplitude

$$|\mathcal{A}|^2 := \sum_{M_i,\lambda_i} |A_{M_i\lambda_i}|^2 \equiv \sum_{M_f,\lambda_f;M_i,\lambda_i} |A^{M_f\lambda_f}_{M_i\lambda_i}|^2. \quad (12)$$

The cross section of Compton scattering of a photon beam with the density matrix $\rho^{(\gamma)}$ from a target with density matrix $\rho^{(\mathrm{d})}$, without detection of the final state polarisations, is then

$$\frac{\mathrm{d}\sigma}{\mathrm{d}\Omega} = \Phi^2 \ \mathrm{tr}[T\rho^{(\mathrm{d})}\rho^{(\gamma)}T^\dagger], \tag{13}$$

where the trace is taken over the polarisation states and Φ is the frame-dependent flux factor, *e.g.*, in the centre-of-mass and lab frames:

$$\Phi_{\mathrm{cm}} = \frac{M_{\mathrm{d}}}{4\pi}\,\frac{1}{\omega_{\mathrm{cm}} + \sqrt{M_{\mathrm{d}}^2 + \omega_{\mathrm{cm}}^2}}\,,$$
$$\Phi_{\mathrm{lab}} = \frac{M_{\mathrm{d}}}{4\pi}\,\frac{1}{M_{\mathrm{d}} + \omega_{\mathrm{lab}}(1-\cos\theta_{\mathrm{lab}})}\,. \tag{14}$$

Transformations between lab and cm kinematics are found in a recent review ([1], sect. 2.3).

By inserting the density matrices of eqs. (6) and (9) into eq. (13), one obtains the cross section in terms of the amplitudes, as function of photon polarisations $P_{\mathrm{circ}}^{(\gamma)}$ and $P_{\mathrm{lin}}^{(\gamma)}$ with polarisation angle φ_{lin} and deuteron polarisation $P_I^{(\mathrm{d})}$ with orientation $(\vartheta_{\mathrm{d}}, \varphi_{\mathrm{d}})$. The functional dependence of the result on these parameters is easily matched to the parametrisation in eq. (10). For the unpolarised part, one finds, of course:

$$\left.\frac{\mathrm{d}\sigma}{\mathrm{d}\Omega}\right|_{\mathrm{unpol}} = \frac{\Phi^2}{6}|\mathcal{A}|^2. \tag{15}$$

The asymmetries are then (these definitions obey the constraints discussed in sect. 2.2)

$$\Sigma^{\mathrm{lin}}\,|\mathcal{A}|^2 = -\sum_{M_i,\lambda_i} A_{M_i\lambda_i} A^*_{M_i,-\lambda_i}, \tag{16}$$

$$T_{IM}\,|\mathcal{A}|^2 = \sqrt{3(2I+1)}\,\mathrm{i}^{\delta_{I1}} \sum_{M_i,M_i',\lambda_i} (-)^{1-M_i} \times \begin{pmatrix} 1 & 1 & I \\ M_i & -M_i' & -M \end{pmatrix} A_{M_i\lambda_i} A^*_{M_i'\lambda_i}, \tag{17}$$

$$T^{\mathrm{circ}}_{IM}\,|\mathcal{A}|^2 = \sqrt{3(2I+1)}\,\mathrm{i}^{\delta_{I2}} \sum_{M_i,M_i',\lambda_i} (-)^{1-M_i}\,\lambda_i \times \begin{pmatrix} 1 & 1 & I \\ M_i & -M_i' & -M \end{pmatrix} A_{M_i\lambda_i} A^*_{M_i'\lambda_i}, \tag{18}$$

$$T^{\mathrm{lin}}_{IM}\,|\mathcal{A}|^2 = \sqrt{3(2I+1)} \sum_{M_i,M_i',\lambda_i} (-)^{-M_i}\,(\mathrm{i}\lambda_i)^{\delta_{I1}}\ \lambda_i^M \times \begin{pmatrix} 1 & 1 & I \\ M_i & -M_i' & -\lambda_i M \end{pmatrix} A_{M_i\lambda_i} A^*_{M_i',-\lambda_i}. \tag{19}$$

These explicit forms can also be used to determine which observables are nonzero only due to inelasticities. Cross sections and, concurrently, the functions Σ^{lin}, T_{IM}, $T^{\mathrm{circ/lin}}_{IM}$ are of course real. The Compton amplitudes $A_{M_i\lambda_i}$ are real below the first inelasticity, so that the occurrence of the imaginary unit in six of the observables in eqs. (16) to (19) indicates that they are zero there, namely below the first inelasticity:

$$T_{11} \equiv 0, \qquad T^{\mathrm{circ}}_{2(1,2)} \equiv 0, \qquad T^{\mathrm{lin}}_{1(0,\pm1)} \equiv 0. \tag{20}$$

2.4 Complete experiments?

The deuteron Compton amplitude contains 2 independent complex amplitudes for a scalar target, 4 more for a vector target, and 6 more for a tensor target (see, *e.g.*, [6]). How many and which of them are accessible with polarised beam and/or target, but without measuring outgoing polarisations (or, by time-reversal invariance, vice versa)? Those which cannot be determined must be probed in polarisation transfer experiments. These are significantly harder because of the difficulties to measure recoil and scattered-photon polarisations.

As a warm-up, one could consider first the Compton scattering below the first inelasticity, where all amplitudes are real. This is however of limited use in deuteron Compton scattering, where the first appreciable breakup process, $\gamma\mathrm{d} \to \mathrm{pn}$, starts at a cm photon energy of $B_{\mathrm{d}} = 2.225\,\mathrm{MeV}$, namely so low that the amplitudes have significant imaginary parts in the experimentally interesting region[3]. In contradistinction, the first appreciable inelasticity on the proton starts at the one-pion production threshold.

Above the first inelasticity, 23 independent real amplitudes exist, namely 3 for a scalar target (2 complex minus an overall phase), 8 more for a vector target, and 12 more for a tensor target. Since the 6 observables of eq. (20) are nonzero there, one finds:

- For scalar targets, only 2 of 3 observables are accessible, leaving 1 to be determined from a polarisation transfer observable.
- For vector polarised targets, 6 of 8 observables are accessible, leaving 2 to be determined from polarisation transfer observables.
- For tensor polarised targets, 10 of 12 observables are accessible, leaving again 2 to be determined from polarisation transfer observables.

The 5 correlations between beam and recoiling target polarisation which are necessary for complete experiments on the deuteron will be discussed in a future publication [15].

This concludes the classification itself; results in χEFT will be presented in sect. 3.3.

2.5 Relation to other parametrisations

Since some observables in Compton scattering with vector and tensor polarised targets have been constructed

[3] The first inelasticity opens at zero energy, with multiple photons in the final state ($\gamma\mathrm{d} \to \gamma\gamma\mathrm{d}$, etc.), but is suppressed by powers of $\alpha = 1/137$ and hence does not significantly contribute in experiments. It is not considered in today's theoretical descriptions, whose first inelasticity thus is the deuteron breakup.

before, it is appropriate to relate these to the classification in eq. (10). Often, observables are expressed not in terms of the degrees of deuteron vector and tensor polarisations, but via the occupation numbers $p_{\pm,0}$ of a state quantised along $\vec{d}$. From eq. (7), the density matrix of a pure deuteron state $|M_{\vec{d}}\rangle$ is

$$\begin{aligned} p_\pm = 1\text{:}\quad & \rho^{(\mathrm{d})}_{\vec{d}} = |M_{\vec{d}}=\pm1\rangle\langle M_{\vec{d}}=\pm1| \\ & \Longleftrightarrow P^{(\mathrm{d})}_1 = \pm\sqrt{\frac{3}{2}} \text{ and } P^{(\mathrm{d})}_2 = \frac{1}{\sqrt{2}} \\ p_0 = 1\text{:}\quad & \rho^{(\mathrm{d})}_{\vec{d}} = |M_{\vec{d}}=0\rangle\langle M_{\vec{d}}=0| \\ & \Longleftrightarrow P^{(\mathrm{d})}_1 = 0 \quad \text{and } P^{(\mathrm{d})}_2 = -\sqrt{2}. \end{aligned} \tag{21}$$

2.5.1 Chen's tensor-polarised cross section [11]

The first tensor observable was constructed by Chen [11], and also used by Karakowski and Miller [12,13]. His definition of a cross section combination for an unpolarised beam on a deuteron which is tensor polarised along the z-axis translates into the observables of eq. (10) with $P^{(\gamma)}_{\mathrm{circ}} = P^{(\gamma)}_{\mathrm{lin}} = 0$, $\vartheta_\mathrm{d} = \varphi_\mathrm{d} = 0$ and eq. (21) into

$$\begin{aligned} \frac{\mathrm{d}\sigma^{[11]}_2}{\mathrm{d}\Omega} := \frac{1}{4}\Big[2\frac{\mathrm{d}\sigma}{\mathrm{d}\Omega}(M_{iz}=0) - \frac{\mathrm{d}\sigma}{\mathrm{d}\Omega}(M_{iz}=1) \\ - \frac{\mathrm{d}\sigma}{\mathrm{d}\Omega}(M_{iz}=-1)\Big] = -\frac{3}{2\sqrt{2}}\,T_{20}\,\frac{\mathrm{d}\sigma}{\mathrm{d}\Omega}\Big|_{\mathrm{unpol}}, \end{aligned} \tag{22}$$

where the subscript in M_{iz} denotes that $\vec{d}$ points along the z-axis for the initial state. From now on, the bracketed superscript of an observable indicates the bibliographic reference from which the notation is taken *verbatim*.

This is the only tensor observable for which calculations exist, namely at 49 and 69 MeV both by Chen and by Karakowski and Miller. Nonetheless, these will not be compared in detail with those of the χEFT approach taken in sect. 3.3. Chen's ones are derived in "pion-less" EFT, *i.e.* for typical momenta well below the pion mass and typical photon energies $\omega \lesssim m_\pi^2/M \approx 20\,\mathrm{MeV}$ [1]. These predictions are thus more of qualitative interest. Shape and size of the angular dependence differ indeed considerably from those presented later. Karakowski and Miller used an approach similar to that which will be outlined in sect. 3.1, but without a dynamical $\Delta(1232)$ and without some pion-exchange diagrams dictated by chiral symmetry [12,13]. Their results at 49 and 69 MeV agree up to about 30% in shape and magnitude with the ones presented below. The difference does not stem from the $\Delta(1232)$, but may be attributed to the fact that their photon-nucleon interaction for rescattering terms is expanded only to first order, while Hildebrandt *et al.* demonstrated that terms up to $l = 2$ should be kept for convergence [35,36]. Tensor observables should be more susceptible to this difference.

2.5.2 Scalar and vector target observables by Babusci *et al.* [5]

Babusci *et al.* [5] were the first to identify a complete set of independent observables for Compton scattering, namely for a spin-$\frac{1}{2}$ target. Their classification applies of course also to a scalar- or vector-polarised deuteron target, *provided* one sets the tensor component to zero, $P^{(\mathrm{d})}_2 \equiv 0$. Following the discussion in sect. 2.1, this constrains $|P^{(\mathrm{d})}_1| \leq \sqrt{\frac{2}{3}}$, so the vector polarisation cannot reach the maximal value of 1 allowed for a spin-$\frac{1}{2}$ target. While one should be aware of this difference, we choose in the following to quote results with a pretense value "$P^{(\mathrm{d})}_1 = 1$". Those for a deuteron target which is maximally vector polarised but not tensor polarised are obtained from these by multiplying the right-hand sides of eqs. (24)–(29) by $\sqrt{\frac{2}{3}}$.

Experimentally, these observables are measured as asymmetries between cross sections with different target and beam polarisation angles $(\vartheta_\mathrm{d}, \varphi_\mathrm{d}; \varphi_\mathrm{lin})$, normalised to their sum. The configurations are chosen such that their cross sections sum to twice the total unpolarised cross section.

Specifically, the beam asymmetry in refs. [5, 8–10] is the difference of the cross sections of a linearly polarised beam ($P^{(\gamma)}_{\mathrm{lin}} = 1$, $P^{(\gamma)}_{\mathrm{circ}} = 0$) either in the scattering plane ($\varphi_\mathrm{lin} = 0$) or perpendicular to it ($\varphi_\mathrm{lin} = \pi/2$) on an unpolarised target ($P^{(\mathrm{d})}_1 = P^{(\mathrm{d})}_2 = 0$), normalised to their sum. Inserting these choices into eq. (10) identifies

$$\begin{aligned} \Sigma^{[5]}_3 \equiv \Sigma^{[8,9]} \equiv \mathit{\Pi}^{\text{lin }[10]} &= \frac{\frac{\mathrm{d}\sigma}{\mathrm{d}\Omega}(\varphi_\mathrm{lin}=0) - \frac{\mathrm{d}\sigma}{\mathrm{d}\Omega}(\varphi_\mathrm{lin}=\frac{\pi}{2})}{\frac{\mathrm{d}\sigma}{\mathrm{d}\Omega}(\varphi_\mathrm{lin}=0) + \frac{\mathrm{d}\sigma}{\mathrm{d}\Omega}(\varphi_\mathrm{lin}=\frac{\pi}{2})} \\ &\equiv \frac{(\varphi_\mathrm{lin}=0)-(\varphi_\mathrm{lin}=\frac{\pi}{2})}{(\varphi_\mathrm{lin}=0)+(\varphi_\mathrm{lin}=\frac{\pi}{2})} \equiv \frac{(\varphi_\mathrm{lin}=0)-(\varphi_\mathrm{lin}=\frac{\pi}{2})}{\cdot+\cdot} \\ &= \Sigma^{\mathrm{lin}}. \end{aligned} \tag{23}$$

For readability, the differential cross section symbol is dropped in each term in the second line, and an abbreviation "$\cdot+\cdot$" is introduced for a denominator which is the sum, rather than the difference, of the terms in the numerator. Not surprisingly, all definitions of the beam asymmetry coincide.

The vector target asymmetry with unpolarised beam ($P^{(\mathrm{d})}_1 = 1$, $P^{(\mathrm{d})}_2 = P^{(\gamma)}_{\mathrm{circ}} = P^{(\gamma)}_{\mathrm{lin}} = 0$) translates as

$$\begin{aligned} \Sigma^{[5]}_y &= \frac{(\vartheta_\mathrm{d}=\frac{\pi}{2}, \varphi_\mathrm{d}=+\frac{\pi}{2}) - (\vartheta_\mathrm{d}=\frac{\pi}{2}, \varphi_\mathrm{d}=-\frac{\pi}{2})}{\cdot+\cdot} \\ &= -\frac{1}{\sqrt{2}}\,T_{11}, \end{aligned} \tag{24}$$

the vector target asymmetries with right circularly polarised beam ($P^{(\mathrm{d})}_1 = 1$, $P^{(\gamma)}_{\mathrm{circ}} = 1$, $P^{(\mathrm{d})}_2 = P^{(\gamma)}_{\mathrm{lin}} = 0$) as

$$\begin{aligned} \Sigma^{[5]}_{2x} &= \frac{(\vartheta_\mathrm{d}=\frac{\pi}{2}, \varphi_\mathrm{d}=0) - (\vartheta_\mathrm{d}=\frac{\pi}{2}, \varphi_\mathrm{d}=\pi)}{\cdot+\cdot} \\ &= -\frac{1}{\sqrt{2}}\,T^{\mathrm{circ}}_{11}, \end{aligned} \tag{25}$$

$$\Sigma^{[5]}_{2z} = \frac{(\vartheta_\mathrm{d}=0) - (\vartheta_\mathrm{d}=\pi)}{\cdot+\cdot} = T^{\mathrm{circ}}_{10}, \tag{26}$$

$$\Sigma_{1x}^{[5]} = \frac{(\vartheta_\mathrm{d}=\frac{\pi}{2},\varphi_\mathrm{d}=0;\varphi_\mathrm{lin}=+\frac{\pi}{4}) - (\frac{\pi}{2},0;\varphi_\mathrm{lin}=-\frac{\pi}{4})}{\cdot+\cdot} = \frac{1}{\sqrt{2}}\left(T_{11}^\mathrm{lin} - T_{1,-1}^\mathrm{lin}\right), \tag{27}$$

$$\Sigma_{1z}^{[5]} = \frac{(\vartheta_\mathrm{d}=0;\varphi_\mathrm{lin}=+\frac{\pi}{4}) - (0;\varphi_\mathrm{lin}=-\frac{\pi}{4})}{\cdot+\cdot} = -T_{10}^\mathrm{lin}, \tag{28}$$

$$\Sigma_{3y}^{[5]} = \frac{[(\vartheta_\mathrm{d}=\frac{\pi}{2},\varphi_\mathrm{d}=\frac{\pi}{2};\varphi_\mathrm{lin}=0) - (\frac{\pi}{2},\frac{\pi}{2};\frac{\pi}{2})] - [(\frac{\pi}{2},-\frac{\pi}{2};0) - (\frac{\pi}{2},-\frac{\pi}{2};\frac{\pi}{2})]}{[\cdot+\cdot]+[\cdot+\cdot]} = -\frac{1}{\sqrt{2}}\left(T_{11}^\mathrm{lin} + T_{1,-1}^\mathrm{lin}\right), \tag{29}$$

and finally those with linearly polarised beam on a vector target ($P_1^{(\mathrm{d})}=1$, $P_\mathrm{lin}^{(\gamma)}=1$, $P_2^{(\mathrm{d})}=P_\mathrm{circ}^{(\gamma)}=0$) as

see eqs. (27)–(29) *above*

or

$$T_{11}^\mathrm{lin} = \frac{1}{\sqrt{2}}\left(\Sigma_{1x}^{[5]} - \Sigma_{3y}^{[5]}\right), \quad T_{1,-1}^\mathrm{lin} = -\frac{1}{\sqrt{2}}\left(\Sigma_{1x}^{[5]} + \Sigma_{3y}^{[5]}\right). \tag{28}$$

For $\Sigma_{2x/z}$, Babusci *et al.* flip the circular beam polarisation. Due to parity symmetry, this is equivalent to flipping the target polarisation above.

2.5.3 Polarised deuteron observables by Chen *et al.* [6], Choudhury/Phillips [8, 9] and Grießhammer/Shukla [10]

These authors define observables in analogy to those introduced by Babusci *et al.* [5]. However, the deuteron is taken to be prepared such that only the magnetic quantum numbers $M_{i\vec{d}} = \pm 1$ contribute, in the direction $\vec{d}$ in which the density matrix is diagonal. To understand why this difference may lead to confusion, consider the single-polarisation observable for scattering an unpolarised (or circularly polarised) beam on a deuteron target which is polarised in a pure $M_{iy} = \pm 1$ state perpendicular to the scattering plane (*i.e.* parallel or anti-parallel to the y-axis),

$$\Sigma_y^{[6]} = \frac{\frac{\mathrm{d}\sigma}{\mathrm{d}\Omega}(M_{iy}=+1) - \frac{\mathrm{d}\sigma}{\mathrm{d}\Omega}(M_{iy}=-1)}{\cdot+\cdot}, \tag{29}$$

where the same abbreviation as in eq. (23) is used. This appears to be the natural application of $\Sigma_y^{[5]}$, eq. (24), to the deuteron. Since the deuteron polarisation is flipped in the difference, the numerator should describe a vector-polarised deuteron. According to eq. (21), a pure state $|M_{i\vec{d}}|=1$ is described by $P_1^{(\mathrm{d})}=\sqrt{3/2}$ and $P_2^{(\mathrm{d})}=1/\sqrt{2}$. For this observable, $\vec{d}$ is parallel to the y-axis, so that $M_{iy}=\pm1$ corresponds to $\vartheta_\mathrm{d}=\pi/2, \varphi_\mathrm{d}=\pm\pi/2$. With $P_\mathrm{circ}^{(\gamma)}=P_\mathrm{lin}^{(\gamma)}=0$ and the same abbreviations as before, the numerator becomes

$$\begin{aligned}(M_{iy}=+1) - (M_{iy}=-1) &= \left(\vartheta_\mathrm{d}=\frac{\pi}{2},\varphi_\mathrm{d}=+\frac{\pi}{2}\right)\\ &- \left(\vartheta_\mathrm{d}=\frac{\pi}{2},\varphi_\mathrm{d}=-\frac{\pi}{2}\right) = -\sqrt{3}\,T_{11}\left.\frac{\mathrm{d}\sigma}{\mathrm{d}\Omega}\right|_\mathrm{unpol}.\end{aligned} \tag{30}$$

Tensor observables do indeed not contribute. In contradistinction, the denominator reads

$$\begin{aligned}&(M_{iy}=+1) + (M_{iy}=-1)\\ &\quad= \left(\vartheta_\mathrm{d}=\frac{\pi}{2},\varphi_\mathrm{d}=+\frac{\pi}{2}\right) + \left(\vartheta_\mathrm{d}=\frac{\pi}{2},\varphi_\mathrm{d}=-\frac{\pi}{2}\right)\\ &\quad= \left[2 - \left(\frac{1}{\sqrt{2}}\,T_{20} + \frac{\sqrt{3}}{2}\,T_{22}\right)\right]\left.\frac{\mathrm{d}\sigma}{\mathrm{d}\Omega}\right|_\mathrm{unpol}.\end{aligned} \tag{31}$$

It is no more proportional to the unpolarised cross section since the $M_{iy}=0$ term is absent, as noted already in refs. [6, 8, 9]. Like in $\Sigma_y^{[5]}$ of eq. (24), the resulting asymmetry,

$$\Sigma_y^{[6]} = -\frac{2\sqrt{3}\,T_{11}}{4-\sqrt{3}\,T_{22}-\sqrt{2}\,T_{20}}, \tag{32}$$

is proportional to T_{11}, but the prefactor has changed and now depends in addition on the tensor-polarised observables $T_{2(0,2)}$. While the same symbol is used for the vector target polarisation in ref. [5] and for that of ref. [6], eq. (29), the two are actually different,

$$\Sigma_y^{[6]} \neq \Sigma_y^{[5]}\,! \tag{33}$$

It is for this reason that the apparent notational degeneracy is lifted throughout this article by including an explicit reference superscript.

Translating the other observables of refs. [6, 8–10] is now straightforward. Asymmetries with unpolarised targets are of course identical, eq. (23). Since ref. [10] considers both differences of polarised cross sections (denoted by $\Delta^{[10]}$) and their asymmetries $\Sigma^{[10]}$, both are also recorded in the following. One finds with $P_1^{(\mathrm{d})}=\sqrt{3/2}$, $P_2^{(\mathrm{d})}=1/\sqrt{2}$, $P_\mathrm{circ}^{(\gamma)}=1$ and $P_\mathrm{lin}^{(\gamma)}=0$ for the asymmetries built in analogy to $\Sigma_{2x/z}^{[5]}$:

$$\begin{aligned}\Delta_x^{\mathrm{circ}\ [10]} &= (M_{ix}=+1;\lambda_i=1) - (M_{ix}=-1;1)\\ &= \left(\vartheta_\mathrm{d}=\frac{\pi}{2},\varphi_\mathrm{d}=0\right) - \left(\frac{\pi}{2},\varphi_\mathrm{d}=\pi\right)\\ &= -\sqrt{3}\,T_{11}^\mathrm{circ}\left.\frac{\mathrm{d}\sigma}{\mathrm{d}\Omega}\right|_\mathrm{unpol},\end{aligned} \tag{34}$$

$$\begin{aligned}\Sigma_x^{\mathrm{circ}\ [10]} &\equiv \Sigma_x^{[6,8,9]} = \frac{\Delta_x^{\mathrm{circ}\ [10]}}{\cdot+\cdot}\\ &= -\frac{2\sqrt{3}\,T_{11}^\mathrm{circ}}{4+\sqrt{3}\,T_{22}-\sqrt{2}\,T_{20}},\end{aligned} \tag{35}$$

$$\begin{aligned}\Delta_z^{\mathrm{circ}\ [10]} &\equiv 2\left[\Delta_1\frac{\mathrm{d}\sigma}{\mathrm{d}\Omega}\right]^{[6]}\\ &= (M_{iz}=+1;1) - (M_{iz}=-1;1)\\ &= (\vartheta_\mathrm{d}=0) - (\vartheta_\mathrm{d}=\pi)\\ &= \sqrt{6}\,T_{10}^\mathrm{circ}\left.\frac{\mathrm{d}\sigma}{\mathrm{d}\Omega}\right|_\mathrm{unpol},\end{aligned} \tag{36}$$

$$\Sigma_z^{\mathrm{circ}\ [10]} \equiv \Sigma_z^{[8,9]} \equiv -\Sigma_z^{[6]} = \frac{\Delta_z^{\mathrm{circ}\ [10]}}{\cdot+\cdot} = \frac{\sqrt{3}\,T_{10}^\mathrm{circ}}{\sqrt{2}+T_{20}}. \tag{37}$$

In no case is the denominator just proportional to the unpolarised cross section; instead, it also depends on $T_{2(0,\pm2)}$. It should be noted that ref. [6] provides formulae for the denominators of $\Sigma^{[6]}_{x/y/z}$ which depend only on the scalar and vector parts of the target polarisation. These results could not be reproduced.

The following additional cross section differences and asymmetries for linearly polarised beam on a polarised deuteron target were described in ref. [10]:

$$\begin{aligned}\Delta_x^{\text{lin }[10]} &= (M_{ix}=1;\varphi_{\text{lin}}=0) - \left(M_{ix}=1;\varphi_{\text{lin}}=\frac{\pi}{2}\right)\\ &= \left(\vartheta_{\text{d}}=\frac{\pi}{2},\varphi_{\text{d}}=0;\varphi_{\text{lin}}=0\right) - \left(\frac{\pi}{2},0;\frac{\pi}{2}\right)\\ &= \left[2\,\Sigma^{\text{lin}} + \frac{\sqrt{3}}{2}\left(T_{22}^{\text{lin}}+T_{2,-2}^{\text{lin}}\right) - \frac{1}{\sqrt{2}}\,T_{20}^{\text{lin}}\right]\left.\frac{\text{d}\sigma}{\text{d}\Omega}\right|_{\text{unpol}}, \quad (38)\end{aligned}$$

$$\begin{aligned}\Sigma_x^{\text{lin }[10]} &= \frac{\Delta_x^{\text{lin }[10]}}{\cdot+\cdot}\\ &= \frac{4\,\Sigma^{\text{lin}} + \sqrt{3}\left(T_{22}^{\text{lin}}+T_{2,-2}^{\text{lin}}\right) - \sqrt{2}\,T_{20}^{\text{lin}}}{4+\sqrt{3}\,T_{22}-\sqrt{2}\,T_{20}}, \quad (39)\end{aligned}$$

$$\begin{aligned}\Delta_z^{\text{lin }[10]} &= (M_{iz}=1;\varphi_{\text{lin}}=0) - \left(M_{iz}=1;\varphi_{\text{lin}}=\frac{\pi}{2}\right)\\ &= (\vartheta_{\text{d}}=0;\varphi_{\text{lin}}=0) - \left(0;\frac{\pi}{2}\right)\\ &= \left[2\,\Sigma^{\text{lin}} + \sqrt{2}\,T_{20}^{\text{lin}}\right]\left.\frac{\text{d}\sigma}{\text{d}\Omega}\right|_{\text{unpol}}, \quad (40)\end{aligned}$$

$$\Sigma_z^{\text{lin }[10]} = \frac{\Delta_z^{\text{lin }[10]}}{\cdot+\cdot} = \frac{2\,\Sigma^{\text{lin}} + \sqrt{2}\,T_{20}^{\text{lin}}}{2+\sqrt{2}\,T_{20}}, \quad (41)$$

with $P_1^{(\text{d})}=\sqrt{3/2}$, $P_2^{(\text{d})}=1/\sqrt{2}$, $P_{\text{circ}}^{(\gamma)}=0$ and $P_{\text{lin}}^{(\gamma)}=1$. Notice that the numerators $\Delta_{x/z}^{\text{lin }[10]}$ depend on different and nontrivial combinations of both Σ^{lin} and $T_{2(0,\pm2)}^{\text{lin}}$. $\Sigma_x^{\text{lin }[10]}$ and $\Sigma_z^{\text{lin }[10]}$ would be identical if the tensor-polarised observables were zero.

The additional terms proportional to $T_{2(0,2)}$ in each denominator of $\Sigma_y^{[6]}$ and $\Sigma_{x/z}^{\text{circ/lin }[10]}$ will by themselves turn out to be rather large, sensitive to the polarisabilities, and significantly dependent on photon energy and scattering angle; see figs. 8, 9 and 11 in sect. 3.3. Without this input, no simple conclusions can thus be drawn on how the sensitivity of $\Sigma_y^{[6]}$ on the polarisabilities translates into the sensitivity of its numerator alone. On the other hand, $\Delta_{x/z}^{\text{lin }[10]}$ is dominated by Σ^{lin} and $T_{2,-2}^{\text{lin}}$ since $T_{2(0,2)}^{\text{lin}}$ will turn out to be very small.

3 Observables in χEFT

3.1 Theoretical ingredients

The following subsections explore the sensitivity of the 18 independent observables to the scalar and spin dipole polarisabilities in χEFT. Since this version of the deuteron Compton scattering amplitudes is described comprehensively in previous publications [10,35,36] and summarised in a recent review [1], its main ingredients are only sketched here.

In χEFT with explicit $\Delta(1232)$ degrees of freedom, four typical low-energy scales are found in deuteron Compton scattering: the pion mass $m_\pi \approx 140\,\text{MeV}$ as the typical chiral scale; the Delta-nucleon mass splitting $\Delta_M \approx 290\,\text{MeV}$; the deuteron binding momentum (inverse deuteron size) $\gamma \approx 45\,\text{MeV}$ as the typical scale of the bound NN system; and the photon energy ω. When measured in units of a natural "high" scale $\Lambda_\chi \gg \Delta_M, m_\pi, \omega, \gamma$ at which χEFT with explicit $\Delta(1232)$ degrees of freedom can be expected to break down because new degrees of freedom become dynamical, each gives rise to a small, dimensionless expansion parameter. Typical values of Λ_χ are the masses of the ω and ρ as the next-lightest exchange mesons (about 700 MeV). To avoid a fourfold expansion, it is convenient to approximately identify some scales so that only one dimensionless parameter is left. In the δ-expansion of Pascalutsa and Phillips [37], one chooses

$$\delta \equiv \frac{\Delta_M}{\Lambda_\chi} \approx \left(\frac{m_\pi}{\Lambda_\chi}\right)^{1/2}, \quad (42)$$

i.e. numerically $\delta \approx 0.4$. The identity is exact for $\Lambda_\chi \approx 600$ MeV. Since present experiments are run at $\omega \lesssim 200\,\text{MeV}$, the nonzero Delta width is not tested, cf. ref. [29].

The two-nucleon dynamics adds the momentum scale γ of the shallow bound state. Based on refs. [10,35,36,38,39], sect. 5 of ref. [1] provides a "unified" deuteron Compton amplitude which is complete at order $e^2\delta^3$ and valid from zero photon energy to just below the pion production threshold, $\omega \lesssim m_\pi$. This variant is identical to $\mathcal{O}(\epsilon^3)$ in the "Small Scale Expansion" [40–43], used in ref. [10]. At this order, the Compton scattering kernel consists of "one-nucleon contributions" in which both photons interact with the same nucleon (fig. 3), and "two-nucleon contributions" (fig. 2). The latter consists of two classes, each of which contributes at the order $\mathcal{O}(e^2\delta^3)$ of the present formulation:

1) Both photons couple to the charged pion-exchange current, fig. 2(a) [44].
2) Each photon couples to the nucleon charge, magnetic moment and/or to different pion-exchange currents (figs. 2(b) and (c)). Between the two couplings, the nucleons rescatter arbitrarily often via the full NN S-matrix (including no rescattering at all). These contributions are small for $\omega \sim m_\pi$ but required for $\omega \lesssim \gamma$ in order to restore the exact low-energy theorem of Compton scattering, *i.e.* the Thomson limit [45–48]. At zero energy, its emergence in the χEFT power counting mandates that the contribution of fig. 2(b) must be exactly minus half that of the one-nucleon Thomson term, fig. 3(a), and that the pion-exchange contributions of fig. 2(a) and (c) must add to zero [1]. Such stringent numerical tests are fulfilled to better than 0.2%. At higher energies, the significance of this

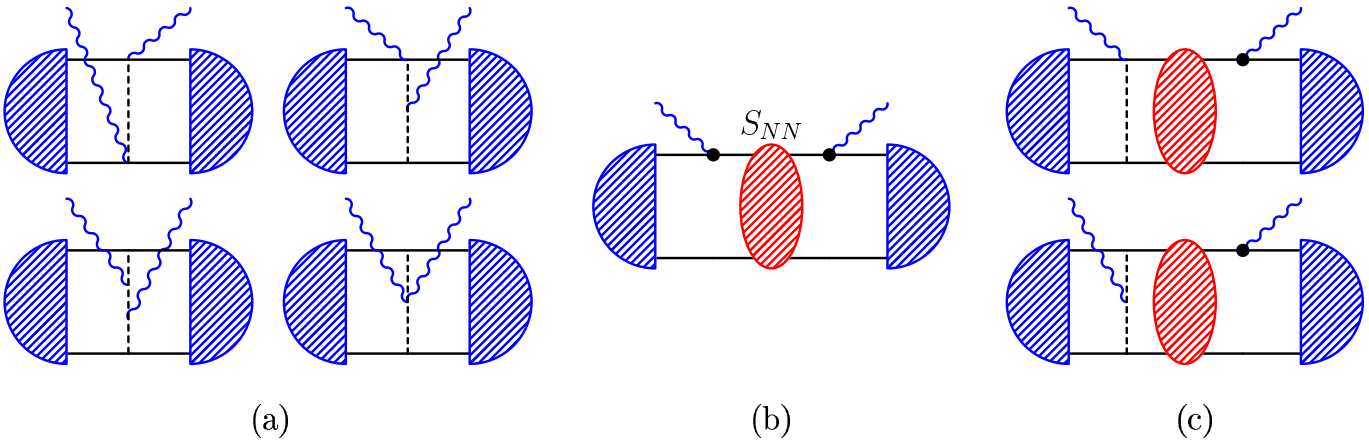

Fig. 2. (Colour on-line) Two-nucleon contributions in χEFT up to order $e^2\delta^3$ (permuted and crossed diagrams not shown). Photons couple to the same pion (a); rescattering contributions (b,c). Ellipse: two-nucleon S-matrix; dot: coupling via minimal substitution or magnetic moment. From ref. [10].

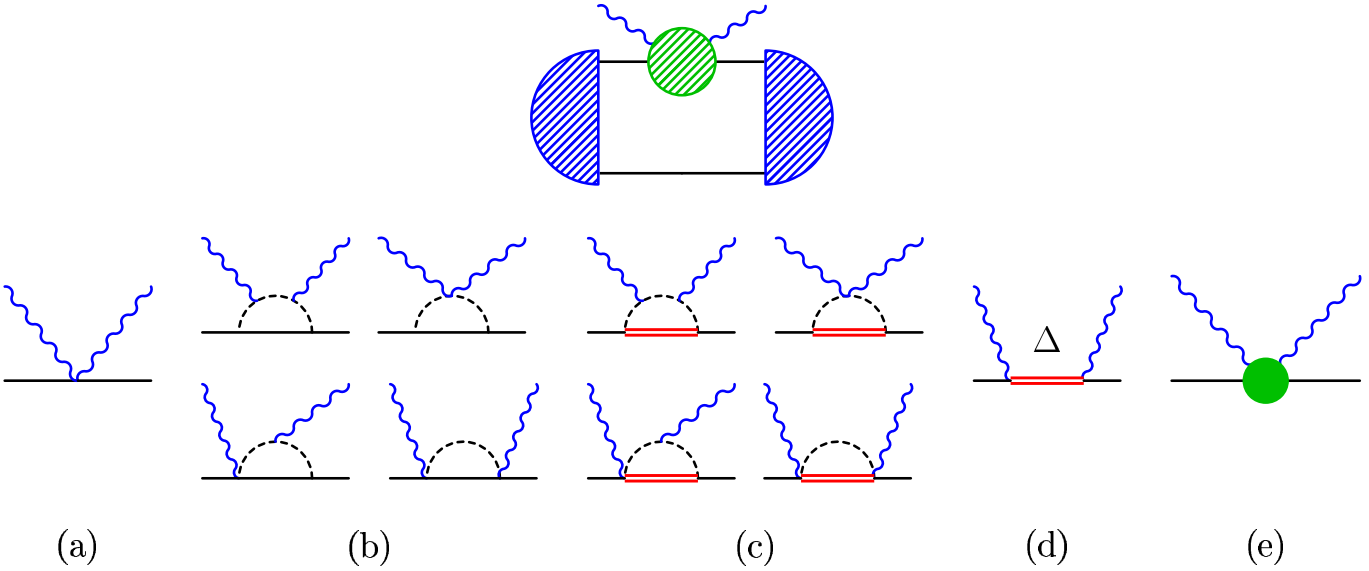

Fig. 3. (Colour on-line) One-nucleon contributions in χEFT up to $\mathcal{O}(e^2\delta^3)$ (permuted and crossed diagrams not shown). Top: embedding into the deuteron. Bottom: one-nucleon Thomson term (a); pion cloud of the nucleon (b) and $\Delta(1232)$ (double line (c)); excitation of an intermediate Δ (d); short-distance effects to α_{E1} and β_{M1} (e). From ref. [10].

cancellation belies in a considerable reduction of the dependence of the amplitudes on the deuteron wave function and NN potential [1].

The one-nucleon sector is formed by:

1) Single-nucleon Thomson scattering, fig. 3(a), is the leading-order term, $\mathcal{O}(e^2\delta^0)$.
2) Coupling to the chiral dynamics of the single-nucleon pion cloud, fig. 3(b), $\mathcal{O}(e^2\delta^2)$.
3) Excitation of the $\Delta(1232)$ intermediate state, fig. 3(d), and coupling to the pion cloud around it, fig. 3(c), each contributing at $\mathcal{O}(e^2\delta^3)$ for $\omega \lesssim m_\pi$. Following ref. [1], Δ is treated nonrelativistically and with zero width, using $\Delta_M = 293\,\mathrm{MeV}$, $g_{\pi\mathrm{N}\Delta} = 1.425$ and the nonrelativistic version of the $\mathrm{N}\Delta\gamma$ $M1$-coupling $b_1 = 5$, obtained from converting the relativistic value of $g_M = 2.9$. This value, in turn, is found by fitting the single-nucleon amplitudes to the data above 150 MeV in the proton Compton database established there.
4) Two energy-independent, isoscalar short-distance coefficients, fig. 3(e), which encode those contributions to the nucleon polarisabilities α_{E1} and β_{M1} which arise at this order neither from pions nor from the $\Delta(1232)$. Since they are formally of one order higher, $\mathcal{O}(e^2\delta^4)$, the order of the resulting total amplitude is called "modified $\mathcal{O}(e^2\delta^3)$". While these "offsets" for the static polarisabilities are determined by data, the energy- and isospin-dependence of the spin-independent polarisabilities are at this order predicted in χEFT. Here, their values are taken from the determination in ref. [1] (see eq. (3)).

Nucleon polarisabilities arise solely from terms 2) to 4). In this power counting, "switching off" $\Delta(1232)$ contributions is equivalent to a calculation at one lower order, $\mathcal{O}(e^2\delta^2)$, in which the scalar polarisabilities are parameter-free predictions: $\alpha_{E1} = 10\beta_{M1} = 12.5$ [27].

These kernels are convoluted with deuteron wave functions to obtain the amplitudes $\langle M_f, \lambda_f | T | M_i, \lambda_i \rangle$ of eq. (11). Results in this article are obtained with the χEFT deuteron wave function at N^{2}LO (cutoff 650 MeV) in the implementation of Epelbaum *et al.* [49] and the AV18 potential [50] for NN rescattering. This combination provides an adequate χEFT representation of the two-nucleon system; see discussion in ref. [1] and sect. 3.3.2 below.

This formulation differs from the previous ones of refs. [10, 35, 36] in some numerical improvements, a new parameter set $(b_1, g_{\pi N\Delta}, \Delta_M)$ for the $\Delta(1232)$ from the Breit-Wigner parameters and the proton Compton data, and in slightly changed numbers for the isoscalar, scalar polarisabilities. In a fully consistent EFT calculation, the kernel, wave functions and potential should of course be derived in the same framework. This is work in progress.

3.2 Strategy

At this (modified) order $e^2\delta^3$, the static isoscalar dipole polarisabilities are (with theoretical uncertainties of about ± 0.8 from higher-order contributions and in the canonical units of $10^{-4}\,\mathrm{fm}^3$ for the scalar polarisabilities and $10^{-4}\,\mathrm{fm}^4$ for the spin-dependent ones) [1, 10, 17]

$$\begin{aligned} \alpha_{E1} &= 10.9, \\ \beta_{M1} &= 3.6, \\ \gamma_{E1E1} &= -5.3, \\ \gamma_{M1M1} &= 3.1, \\ \gamma_{M1E2} &= 0.9, \\ \gamma_{E1M2} &= 0.9, \end{aligned} \tag{43}$$

i.e. $\gamma_0 = +0.4$, $\gamma_\pi = 8.4$, which is not incompatible with those of other approaches, see eq. (5). The values for the spin polarisabilities differ slightly from those quoted in refs. [10, 17] because of the updates to the $\mathcal{O}(e^2\delta^3)$ amplitudes described in sect. 5.3 of the ref. [1]. The convergence of the spin polarisabilities from $\mathcal{O}(e^2\delta^2)$ via the $\mathcal{O}(e^2\delta^3)$ values quoted above to the values at $\mathcal{O}(e^2\delta^4)$ is complicated (see table 4.2 of ref. [1]). Therefore, no theoretical uncertainty is assigned for now.

Since the deuteron is an isoscalar, only average nucleon polarisabilities are accessible in elastic deuteron Compton scattering. In order to analyse the sensitivity of each observable, one varies each dipole polarisability about the static central value by adding the parameters $\delta\alpha_{E1}$, $\delta\beta_{M1}$, $\delta\gamma_{E1E1}$, $\delta\gamma_{M1M1}$, $\delta\gamma_{E1M2}$ and $\delta\gamma_{M1E2}$ to the interactions of the single-nucleon subsystem, eq. (1) [8, 10]. Their contribution to the amplitudes in the γN cm system is

$$\begin{aligned} &A^{\mathrm{fit}}(\omega, z) = \\ &4\pi\,\omega^2 \Big[\left[\delta\alpha_{E1} + z\,\delta\beta_{M1}\right](\vec{\epsilon}\,' \cdot \vec{\epsilon}) - \delta\beta_{M1}\,(\vec{\epsilon}\,' \cdot \hat{k})\,(\vec{\epsilon} \cdot \hat{k}') \\ &-\mathrm{i}[\delta\gamma_{E1E1} + z\delta\gamma_{M1M1} + \delta\gamma_{E1M2} + z\delta\gamma_{M1E2}]\omega\,\vec{\sigma} \cdot (\vec{\epsilon}\,' \times \vec{\epsilon}) \\ &+\mathrm{i}\left[\delta\gamma_{M1E2} - \delta\gamma_{M1M1}\right]\omega\,\vec{\sigma} \cdot \left(\hat{k}' \times \hat{k}\right)(\vec{\epsilon}\,' \cdot \vec{\epsilon}) \\ &+\mathrm{i}\,\delta\gamma_{M1M1}\,\omega\,\vec{\sigma} \cdot \left[\left(\vec{\epsilon}\,' \times \hat{k}\right)(\vec{\epsilon} \cdot \hat{k}') - \left(\vec{\epsilon} \times \hat{k}'\right)(\vec{\epsilon}\,' \cdot \hat{k})\right] \\ &+\mathrm{i}\,\delta\gamma_{E1M2}\,\omega\,\vec{\sigma} \cdot \left[\left(\vec{\epsilon}\,' \times \hat{k}'\right)(\vec{\epsilon} \cdot \hat{k}') - \left(\vec{\epsilon} \times \hat{k}\right)(\vec{\epsilon}\,' \cdot \hat{k})\right]\Big]. \end{aligned} \tag{44}$$

These variables may be considered as parametrising the difference between predicted and (so far unmeasured) experimental static values of the polarisabilities, under the assumption that the energy-dependence from the pion-cloud and $\Delta(1232)$ is correctly predicted in χEFT. Alternatively, one can view them as parametrising deviations from the order-$e^2\delta^3$ χEFT amplitudes at fixed nonzero energy, including the theoretical uncertainties of higher-order effects. In that case, the deviations themselves could be seen as energy-dependent. Such an approach forms the basis of a multipole analysis of deuteron Compton scattering advocated in refs. [10, 39, 51]. Determining the six dipole polarisabilities is then in principle reduced to a multipole analysis of $6 + 1$ high-accuracy scattering experiments.

The variation of the isoscalar values by ± 2 canonical units is chosen since it is roughly at the level of the combined statistical, theoretical and Baldin-sum-rule–induced error for α_{E1} and β_{M1} (3). With quadratic contributions of the polarisabilities $\delta(\alpha_{E1}, \beta_{M1}, \gamma_i)$ suppressed in the squared amplitudes, variations by other amounts are easily linearly extrapolated. In practise, the scalar polarisabilities of the proton are constrained to better than ± 2, so that deuteron Compton scattering experiments are more likely focused on extracting neutron polarisabilities. In that case, these studies can be interpreted as providing the sensitivities on varying the neutron polarisabilities by ± 4 units, with fixed proton values.

The spin polarisabilities are however less well known; besides the constraints of eq. (5), no experimental information has been published thus far, and theoretical descriptions easily disagree by as much as 2 units [1]. For example, a recent determination of the scalar dipole polarisabilities of the proton included varying one of the spin polarisabilities to $\gamma_{M1M1} = 2.2 \pm 0.5(\mathrm{stat})$, which —combined with its theoretical accuracy— would by itself already suggest a variation by about 2 units.

Amplitudes from scalar polarisabilities scale like ω^2, while those containing spin polarisabilities scale like ω^3; see eq. (44). Ideally, one can therefore perform high-accuracy experiments at relatively low energies, $\omega \lesssim 70\,\mathrm{MeV}$, to better determine α_{E1} and β_{M1} and constrain high-energy predictions. The spin polarisabilities are then extracted at $\gtrsim 100\,\mathrm{MeV}$, as already advocated in ref. [10]. The observables considered here follow this pattern.

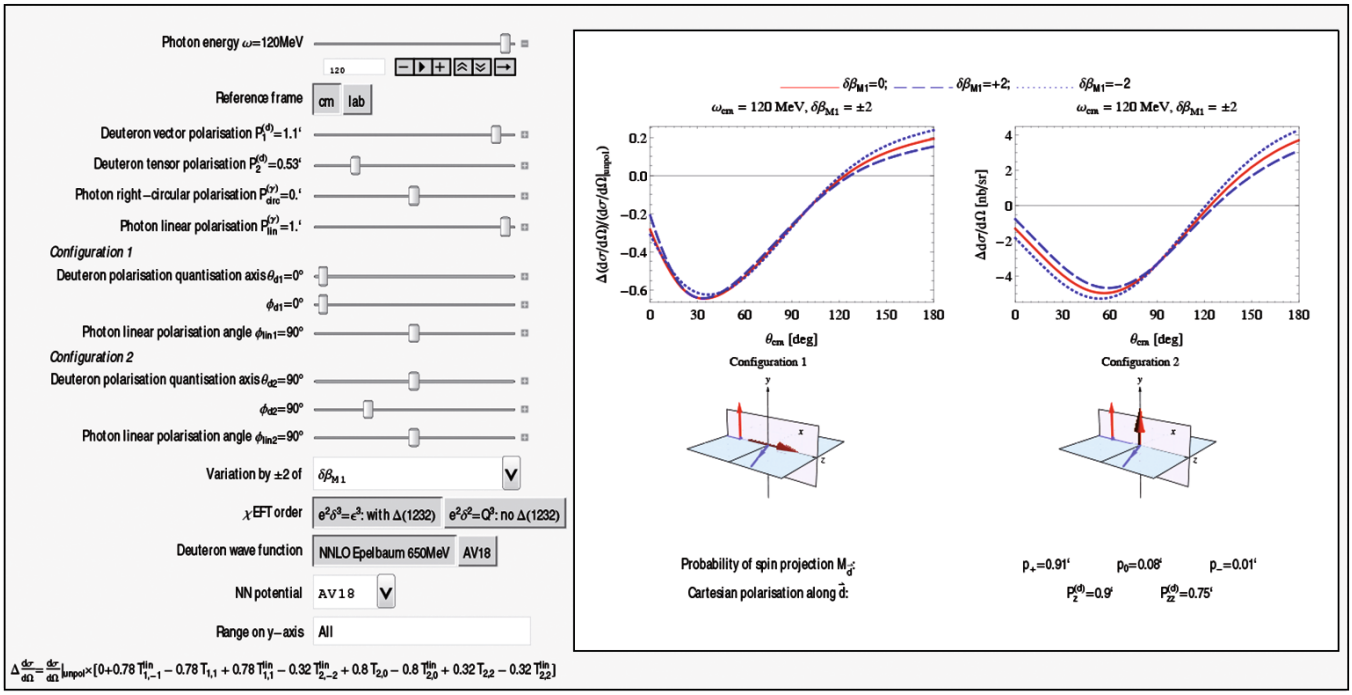

Fig. 4. (Colour on-line) Screenshot of part of the interactive *Mathematica* notebook.

Additionally, one should address:

1) The Baldin sum rule constraint, eq. (4). However, its independent test by better data at forward angles would be expedient.
2) Weaker constraints for the forward and backward spin polarisabilities, eq. (5). These come with considerable theoretical and systematic uncertainties.
3) Logistic constraints like detector placement and available beam energies, as well as detector and polarisation efficiencies. All these must be taken into account to determine which experiments have the potential for the greatest sensitivity on a given polarisability and of the greatest impact in the network of data already available.

Considering asymmetries removes many systematic experimental uncertainties, but the corresponding count rates are necessary for beam-time estimates and follow from multiplying with the unpolarised cross section, cf. (10). In general, asymmetries are by $\lesssim 30\%$ less sensitive to variations of the polarisabilities than the corresponding count rates. Sometimes, sensitivity to the nucleon structure is even lost entirely, while an enhancement appears in no case. It is the purview of our experimental colleagues to determine to what extent such drawbacks outweigh the benefits of measuring asymmetries instead of cross section differences.

To present all 17 asymmetries and their rates, plus the unpolarised cross section, depending on 6 dipole polarisabilities and 2 kinematic variables (photon energy ω and scattering angle θ) in the cm and lab frame, plus additional theoretical uncertainties and both theoretical and experimental constraints, far exceeds what can adequately be conveyed in an article. Here, the focus is therefore on some prominent examples. In order to facilitate planning and analysis of experiments, the results of all observables are available as an interactive *Mathematica 9.0* notebook from `hgrie@gwu.edu`. It contains both tables and plots of energy- and angle-dependencies of the cross sections, rates and asymmetries from 10 to about 120 MeV, in both the cm and lab systems, including sensitivities to varying the scalar and spin polarisabilities independently as well as subject to the Baldin sum rule and other constraints. Since it considers all observables with polarised beams and/or targets, it supersedes ref. [10] which only dealt with some observables, built in analogy to the Babusci classification; see sect. 2.5.3. Figure 4 shows a sample screenshot of a cross section difference with user-defined beam and target polarisations.

It is finally worth re-emphasising that the purpose of this study is to establish *relative sensitivities* of Compton scattering observables on *varying* the polarisabilities [10]. Credible predictions of their absolute magnitudes are only meaningful when all systematic uncertainties are properly propagated into observables. Such errors include: theoretical uncertainties from discarding contributions in χEFT which are higher than order $e^2\delta^3$, like including effects of the $\Delta(1232)$ width and parameter uncertainties; uncertainties in the data and in the Baldin sum rule, eq. (4); and, to a lesser extent, residual dependence on the deuteron wave function and NN potential used, as well as numerical uncertainties.

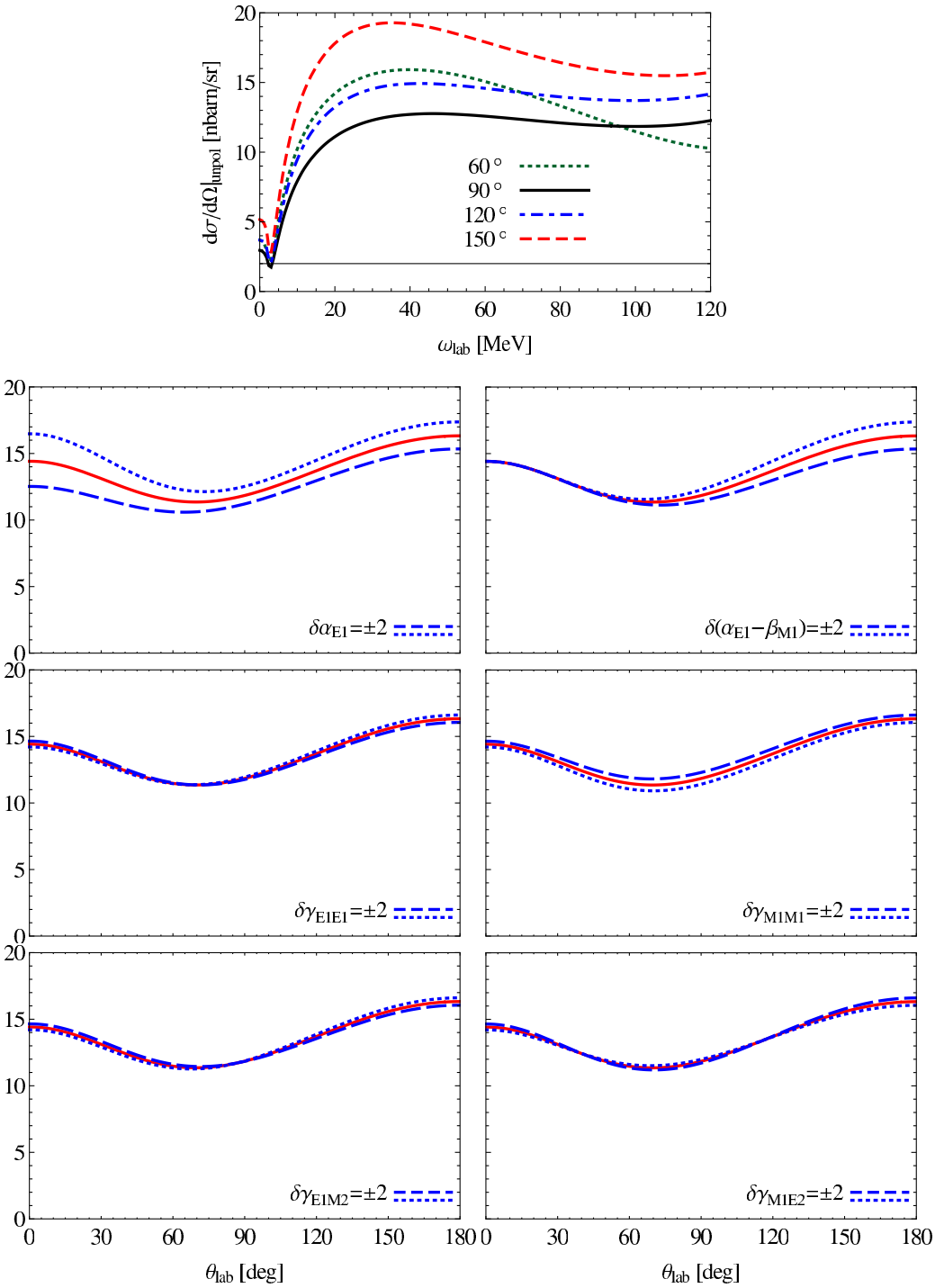

Fig. 5. (Colour on-line) Unpolarised cross section $\mathrm{d}\sigma/\mathrm{d}\Omega|_{\mathrm{unpol}}$ in the lab frame, in nbarn/sr. Top: energy-dependence at different angles. Other panels: sensitivity to varying a polarisability abouts its central value (solid line) of eq. (43) by +2 (dashed line) and −2 (dotted line) units, at $\omega_{\mathrm{lab}} = 100\,\mathrm{MeV}$. From top left to bottom right: variation of α_{E1}, $\alpha_{E1} - \beta_{M1}$ (constrained by the Baldin sum rule), γ_{E1E1}, γ_{M1M1}, γ_{E1M2}, γ_{M1E2}.

3.3 Results

3.3.1 Size and sensitivity

Figures 5 to 23 present the χEFT results of an $\mathcal{O}(e^2\delta^3)$ calculation, with dynamical $\Delta(1232)$ and NN rescattering. Let us concentrate on the sensitivity to the polarisabilities at one representative energy in the (experimentally most relevant) lab frame. With an eye on parameters at HIγS, MAXlab, MAMI and possible future high-luminosity accelerators like MESA [52], a beam energy of $\omega_{\mathrm{lab}} = 100\,\mathrm{MeV}$ seems appropriate. Staying below the pion-production threshold avoids experimental and theoretical complications.

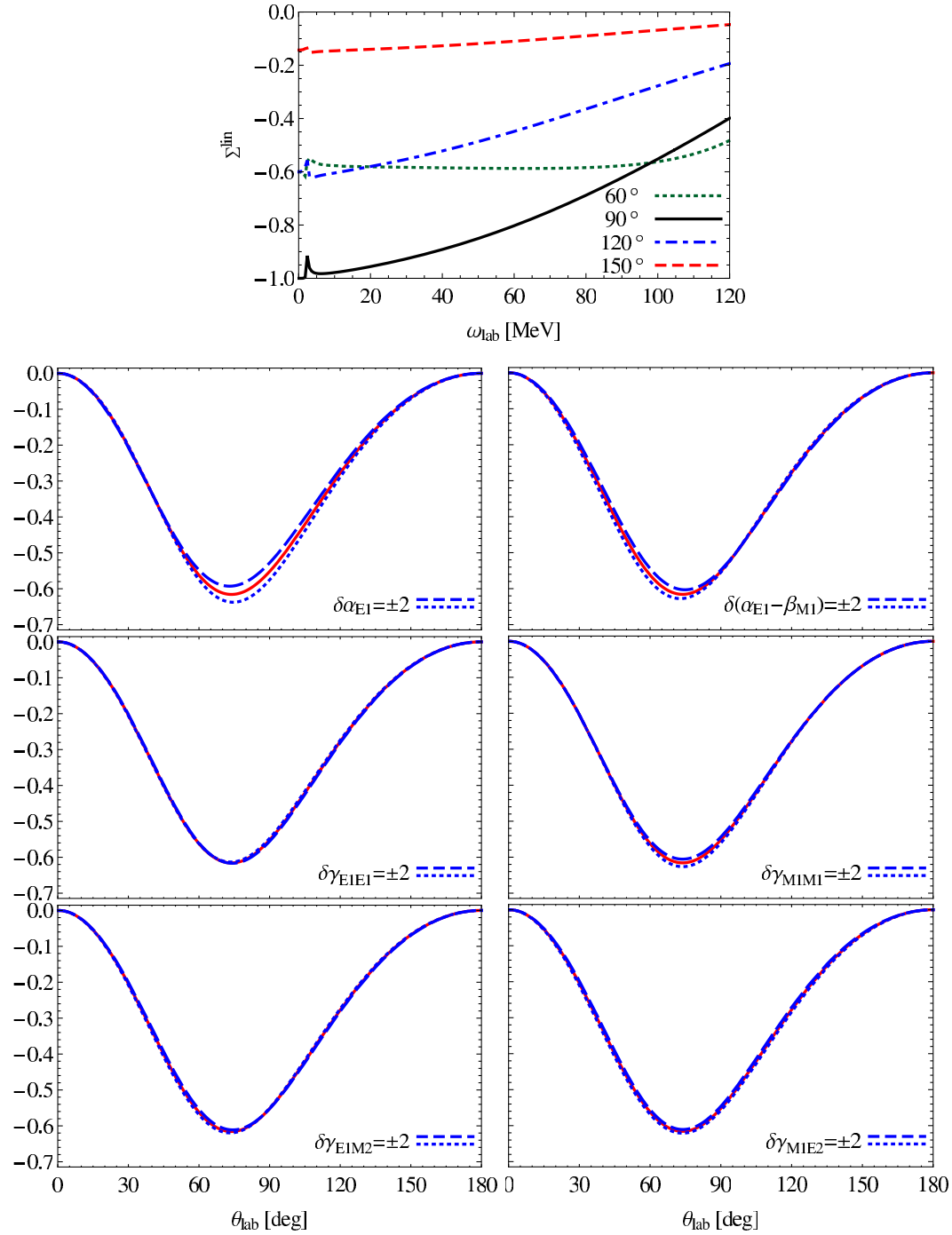

Fig. 6. (Colour on-line) Beam asymmetry $\Sigma^{\rm lin}$ in the lab frame. Top: energy-dependence at different angles. Other panels: sensitivity to varying a polarisability abouts its central value (solid line) of eq. (43) by +2 (dashed line) and −2 (dotted line) units, at $\omega_{\rm lab} = 100\,$MeV. From top left to bottom right: variation of α_{E1}, $\alpha_{E1} - \beta_{M1}$, γ_{E1E1}, γ_{M1M1}, γ_{E1M2}, γ_{M1E2}.

Since the asymmetries differ by 3 orders of magnitude, one should keep in mind changes of scale between plots of different observables. Comparing them is simplified by plots of T_{2M}, $T^{\rm circ}_{1M}$, $T^{\rm circ}_{2M}$, $T^{\rm lin}_{1M}$ and $T^{\rm lin}_{2M}$, each for the different nontrivial values of M at $\omega_{\rm lab} = 100\,$MeV. With magnitudes of up to 0.60, the largest asymmetries are $\Sigma^{\rm lin}$, $T^{\rm circ}_{10}$ and $T^{\rm lin}_{2,-2}$, followed by magnitudes on the order of 0.1 for T_{JM}, $T^{\rm circ}_{11}$, $T^{\rm lin}_{1,(0,-1)}$ and $T^{\rm lin}_{2(0,-1)}$. The order of magnitude of $T^{\rm circ}_{2M}$, $T^{\rm lin}_{10}$ and $T^{\rm lin}_{21}$ is 10^{-2}, and that of $T^{\rm lin}_{11}$ and $T^{\rm lin}_{22}$ even 10^{-3}, providing considerable experimental challenges. The observables $T^{\rm lin}_{JM}$ show a clear hierarchy, with sizes increasing substantially towards the most negative M-values at given J.

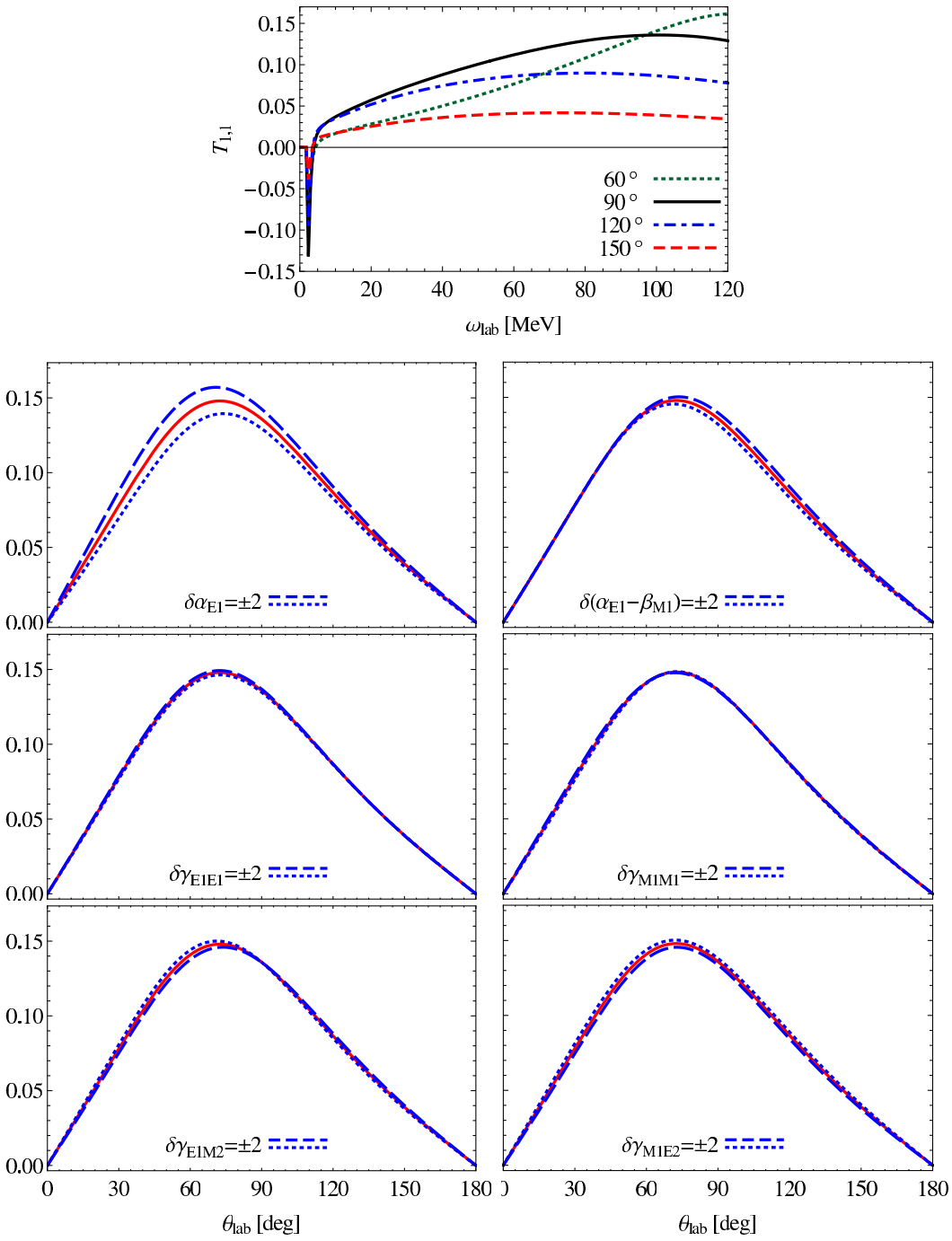

Fig. 7. (Colour on-line) Vector target asymmetry T_{11} (lab frame). See fig. 6 for notes.

The top panel of each single-observable plot, figs. 5 to 7 and 9 to 23, shows the energy-dependence of each observable at four scattering angles $\theta_{\rm lab} \in \{60°; 90°; 120°; 150°\}$. In each case, the deuteron breakup point at $\omega_{\rm lab} \approx 3\,$MeV is clearly visible. Only $T_{22}^{\rm circ}$ and $T_{22}^{\rm lin}$ significantly decrease with increasing photon energy, but $T_{2(1,0)}$ and $T_{20}^{\rm lin}$ change sign around 90 MeV. All observables which are zero below the first threshold, eq. (20), grow rapidly above it —in the case of T_{11} and $T_{1,-1}^{\rm lin}$ even to ≈ 0.2 at 100 MeV.

Sensitivity on the nucleon polarisabilities grows as expected with increasing photon energy. In the lower panels of figs. 5 to 7 and 9 to 23, two plots show the sensitivity to α_{E1} and the combination $\alpha_{E1} - \beta_{M1}$ when the Baldin sum rule constraint is used. This, of course, also allows one to assess where variations of β_{M1} are (anti-)correlated to those of α_{E1}. The other 4 panels describe variations of the spin polarisabilities, without imposing additional constraints. Within one observable, all sensitivities are of course plotted on the same scale.

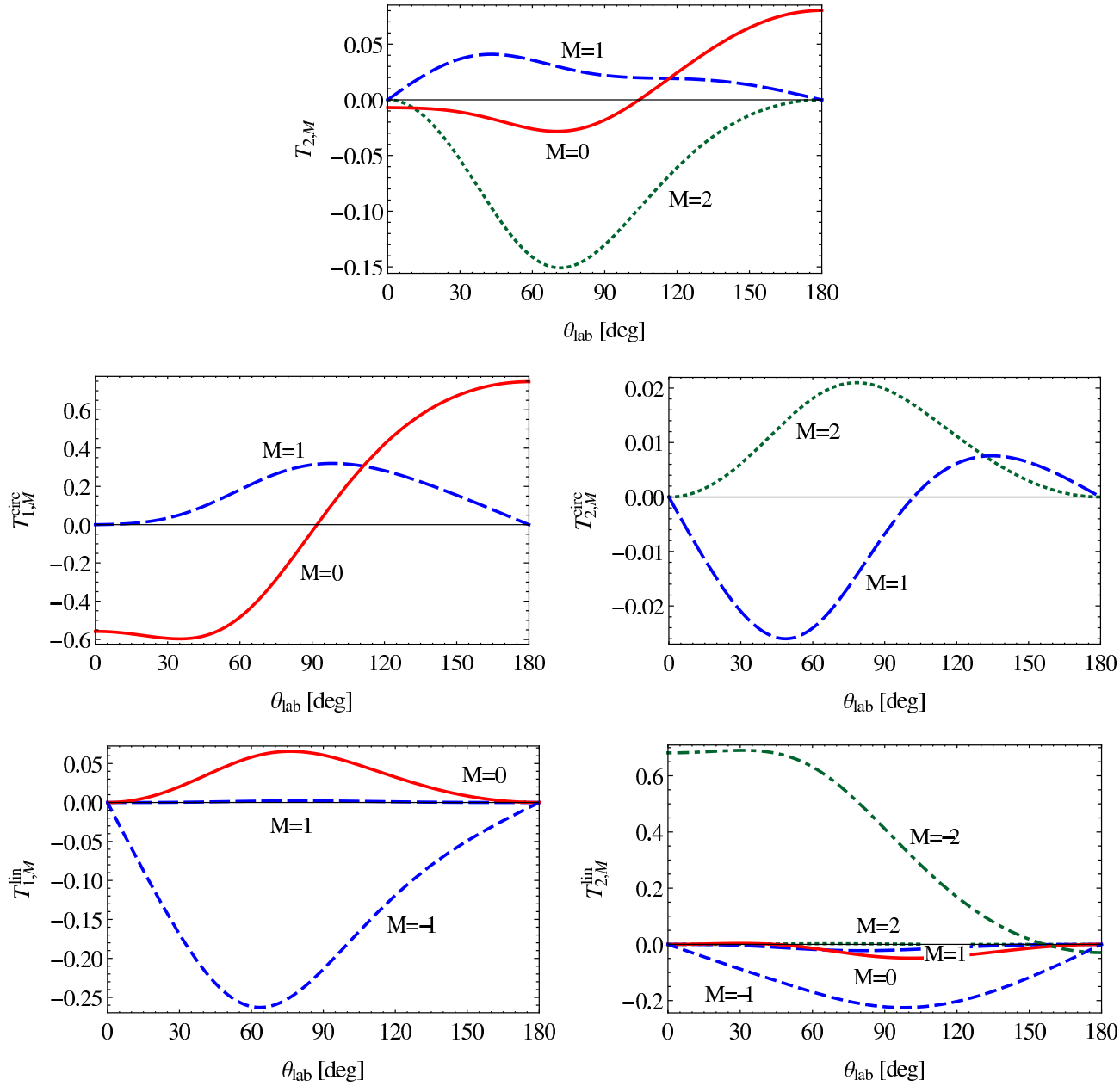

Fig. 8. (Colour on-line) Comparison of the relative sizes of, from top left to bottom right, T_{2M}, $T^{\rm circ}_{1M}$, $T^{\rm circ}_{2M}$, $T^{\rm lin}_{1M}$, $T^{\rm lin}_{2M}$, at $\omega_{\rm lab} = 100\,$MeV in the lab frame, with the static polarisabilities given by eq. (43). solid line: $M = 0$; dashed line: $M = 1$; dotted line: $M = 2$; short-dashed line: $M = -1$; dash-dotted line: $M = -2$. Each panel is drawn at a different scale.

Plots of the unpolarised cross section, fig. 5, are included for quick rate estimates. Its overall size is dramatically affected by a variation of α_{E1}, its backward angles by that of $\alpha_{E1} - \beta_{M1}$, and there is only minor sensitivity on the spin polarisabilities.

The beam asymmetry $\Sigma^{\rm lin}$ shows a mildly different angular dependence on α_{E1} and β_{M1}, possibly allowing for extractions. That sensitivity to the other polarisabilities is small, had already been demonstrated in a χEFT variant without dynamical $\Delta(1232)$ in refs. [8, 9]. Delta effects affect this variable only minimally.

In a future world of high-accuracy experiments with well-controlled systematic experimental uncertainties, high luminosities and 100% beam and target polarisations, an ideal observable should be very sensitive to one polarisability, while being near insensitive to all others. For α_{E1}, this singles out T_{11} (fig. 7), $T^{\rm lin}_{1,-1}$ (fig. 18) and $T^{\rm lin}_{2,-2}$ (fig. 23); for γ_{E1E1}, $T^{\rm circ}_{11}$ (fig. 12). When one takes α_{E1} and β_{M1} to be know sufficiently well that the influence on varying them can be neglected, then $T^{\rm circ}_{11}$ (fig. 12), $T^{\rm circ}_{2(2,1)}$ (figs. 14 and 15) and $T^{\rm lin}_{10}$ (fig. 17) are dominated by sensitivity to γ_{E1E1} only. Curiously, $T^{\rm lin}_{11}$ (fig. 16) is near exclusively sensitive to the mixed spin polarisability γ_{M1E2}, and both $T^{\rm lin}_{22}$ (fig. 19) and $T^{\rm lin}_{21}$ (fig. 20) to its partner γ_{E1M2} —albeit all three are very small.

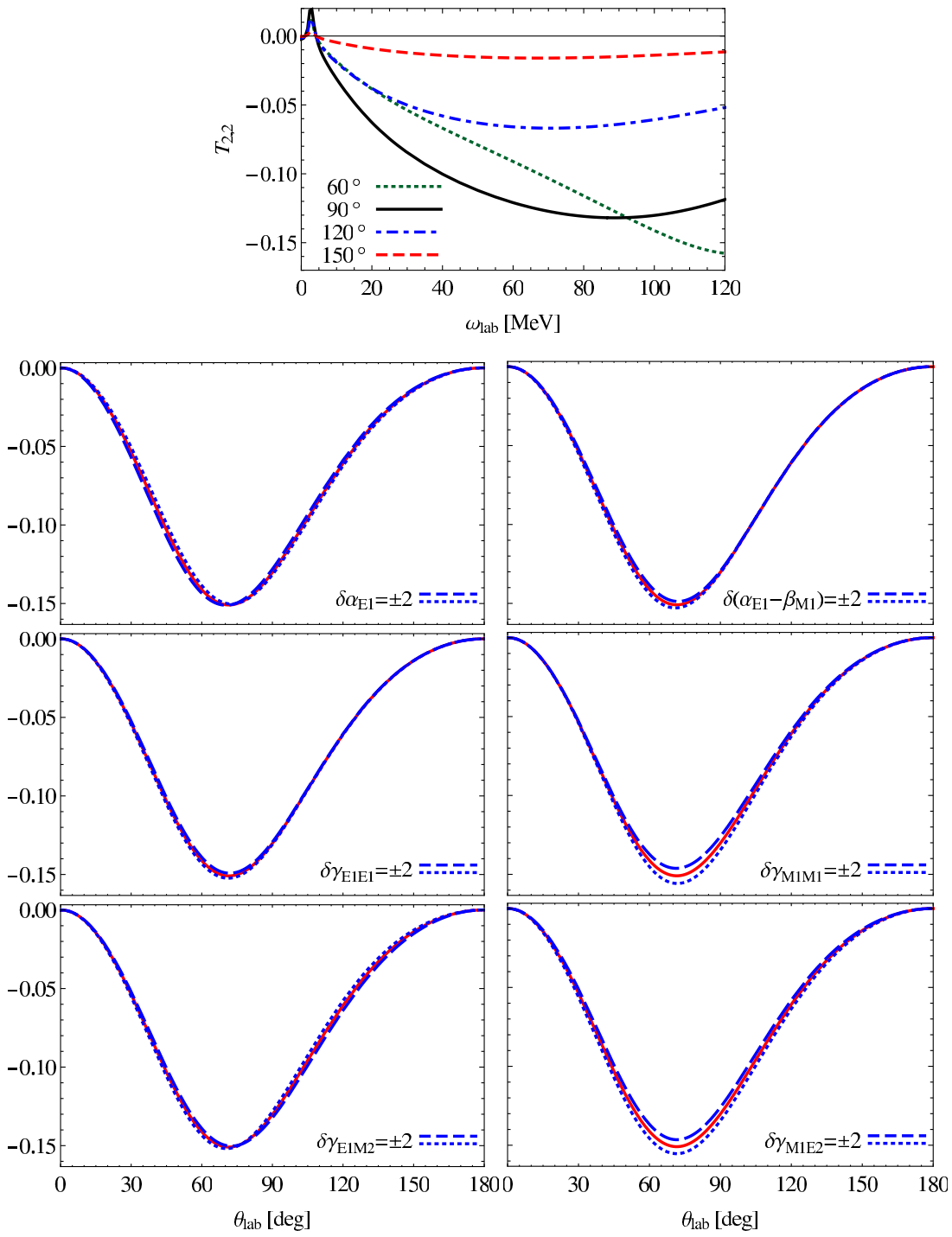

Fig. 9. (Colour on-line) Tensor target asymmetry T_{22} (lab frame). See fig. 6 for notes.

Alternatively, different angular dependencies can be used to disentangle two polarisabilities from the same observable; see, *e.g.*, T_{21} for γ_{E1E1} and γ_{M1E2} (fig. 10) and —to a lesser extent— $T_{20}^{\rm lin}$ for γ_{M1M1} and γ_{E1M2} (fig. 21). Keeping in mind that none of the tensor observables have an analogue in Compton scattering off the nucleon, such an augmentation is absent in the one-nucleon case. It appears that mixed polarisabilities are much better accessible in scattering from the deuteron. The photon quadrupole coupling to one nucleon ($M2$ in γ_{E1M2} and $E2$ in γ_{M1E2}) seems to be enhanced by the D wave components of the deuteron wave function and pion-exchange current, fig. 2(a) and (c). One may thus speculate that determinations of γ_{E1M2} and γ_{M1E2} will first appear from deuteron data —if the necessary accuracy can be reached for these small asymmetries.

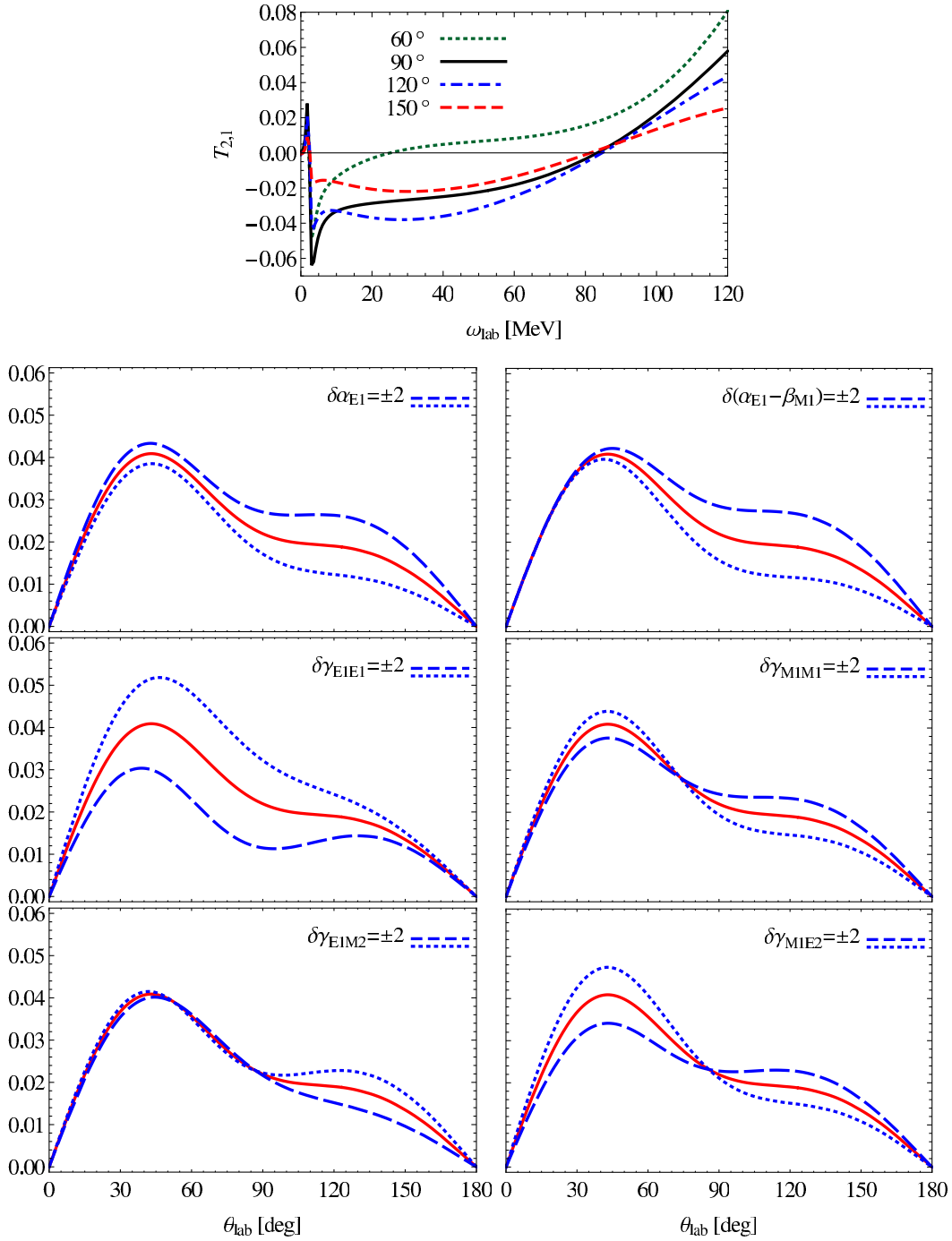

Fig. 10. (Colour on-line) Tensor target asymmetry T_{21} (lab frame). See fig. 6 for notes.

References [1, 10, 53] have argued in detail that sensitivity to a specific polarisability can be maximised or switched off by considering particular target-beam combinations at particular angles. To that end, one either maximises the scalar products between photon polarisations $\vec{\epsilon}$, $\vec{\epsilon}\,'$, photon momenta $\vec{k}$, $\vec{k}'$ and nucleon spin $\vec{\sigma}$, or one chooses some vectors to be orthogonal or parallel, rendering the associated (scalar or vector) products zero. Many of these "zero-sensitivity points" are preserved when the relative motion of the γN cm system inside the deuteron is taken into account. In some cases, the deuteron effect lifts the zero, but only barely, since the nucleons are predominantly in a relative S wave, while D wave contributions (also from pion-exchange currents, fig. 2(a–c)) are suppressed. Relativistic boost effects are small at the energies considered [54]. Examples include the following insensitivities (angles in the cm frame): $T_{2(2,0)}$ to β_{M1} at 90°; T_{20} to γ_{E1E1} at 60° and to γ_{E1M2} at 120°; T_{21} to γ_{E1M2} and γ_{M1E2} at 90°; $T_{21}^{\rm circ}$ to γ_{E1E1} at 90°; and $T_{2,-1}^{\rm lin}$ to γ_{M1M1} at 90°.

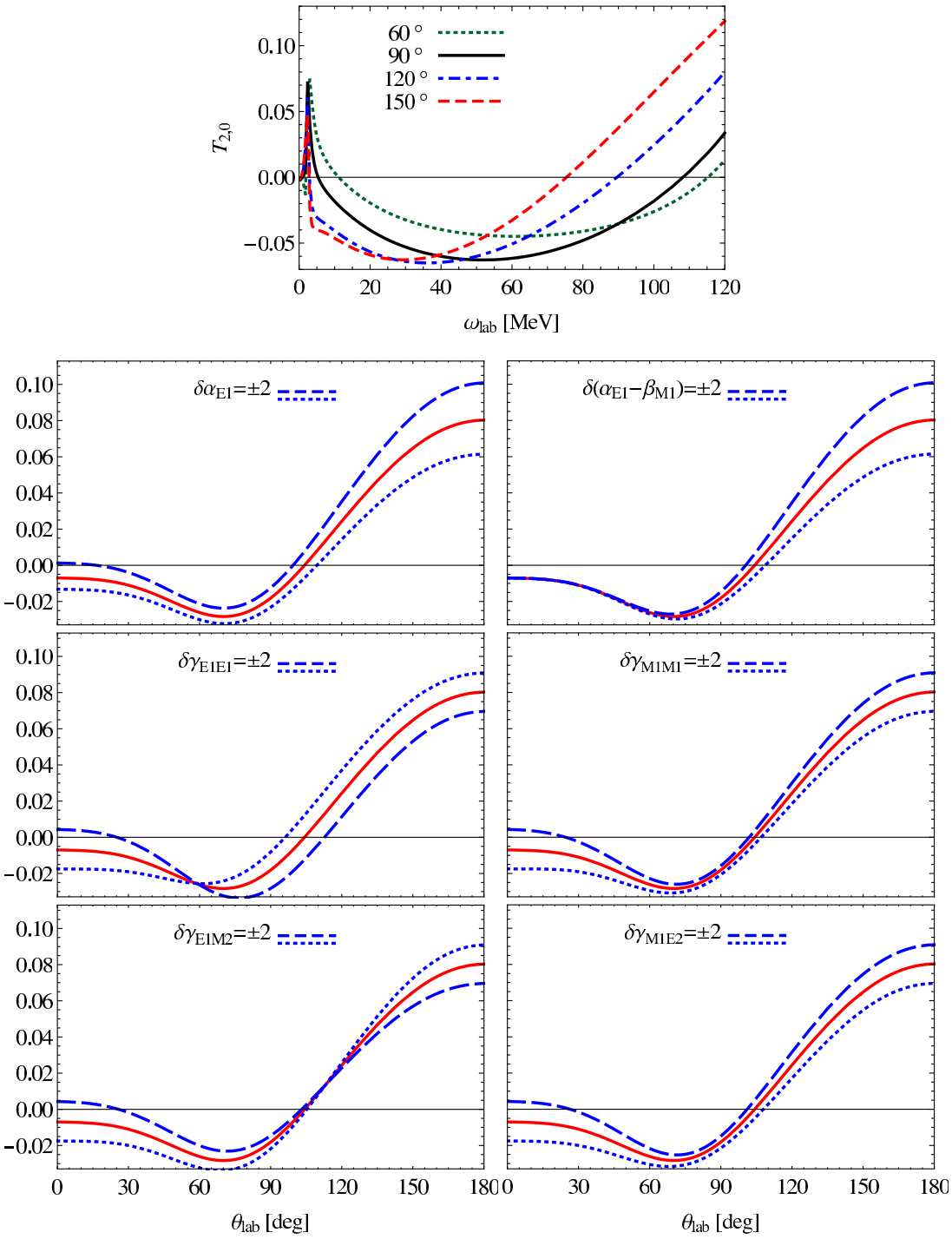

Fig. 11. (Colour on-line) Tensor target asymmetry T_{20} (lab frame). See fig. 6 for notes.

A good example of undesired correlations between variations of different polarisabilities is $T_{22}^{\rm circ}$ (fig. 14), where angular dependencies and magnitudes of changing α_{E1} and γ_{E1E1} are near identical. $T_{10}^{\rm circ}$ (fig. 13) is near equally sensitive to all dipole polarisabilities.

Applying these criteria and assuming that α_{E1} and β_{M1} are known, the following observables could therefore provide an experimentally realistic but challenging complete set from which to cleanly determine the isoscalar spin polarisabilities: $T_{11}^{\rm circ}$ for γ_{E1E1} (variation by ±2 translates into ±5% of an asymmetry magnitude of about 0.3), followed by angular dependence of $T_{20}^{\rm lin}$ (±15% of mag. 0.05) for γ_{M1M1}, followed by T_{22} (±5% of mag. 0.15) for γ_{M1E2} and check on γ_{M1M1}, plus $T_{21}^{\rm lin}$ (±15% of mag. 0.03) for γ_{E1M2}. The different angular dependencies of T_{21} (up to ±20% of mag. 0.05) can serve as valuable check.

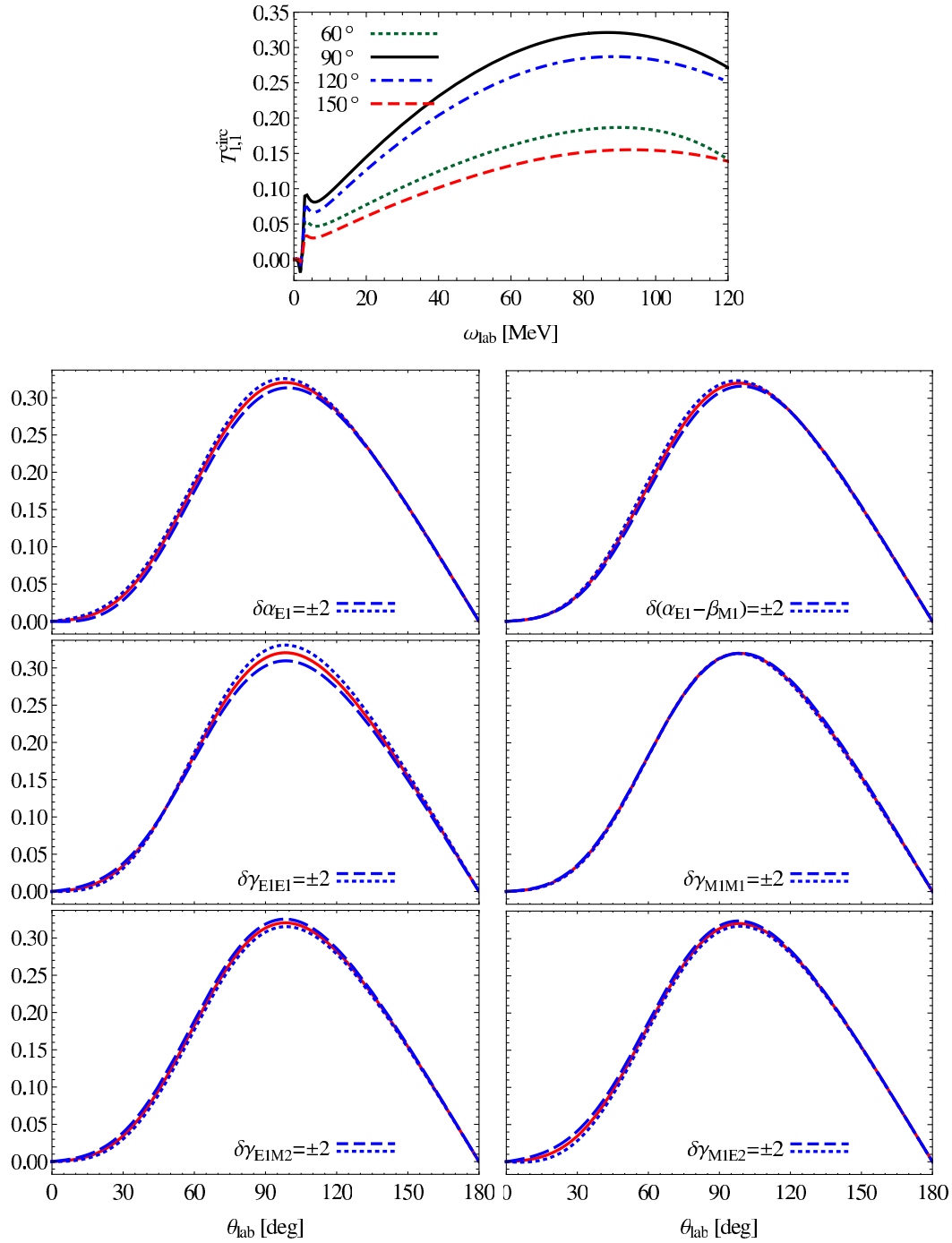

Fig. 12. (Colour on-line) Double asymmetry $T_{11}^{\rm circ}$ (lab frame). See fig. 6 for notes.

3.3.2 Dependence on rescattering, Δ-physics and the NN interaction

As hinted above, reliable theoretical predictions should include a study of residual theoretical uncertainties. The aforementioned *Mathematica* notebook therefore explores the influence of NN rescattering, of the dynamical $\Delta(1232)$, and of the particular two-nucleon interaction used. The results mostly confirm those of refs. [1,10] and thus are only summarised here. Rescattering significantly affects all observables for energies $\lesssim 70$ MeV and is important to reduce residual dependence on the NN potential and deuteron wave function up to 120 MeV, as predicted by the power counting. Details of the NN potential or deuteron wave function are not reflected in observables. For example, at 100 MeV, the largest wave function dependencies are $\approx \pm 5\%$ of the maximum in $T_{22}^{\rm circ}$ and $\approx \pm 2\%$ of the maximum in $T_{20}^{\rm lin}$. These observables are however quite small (< 0.05); all other observables suffer from a residual wave function dependence of $< 1\%$ at that en-

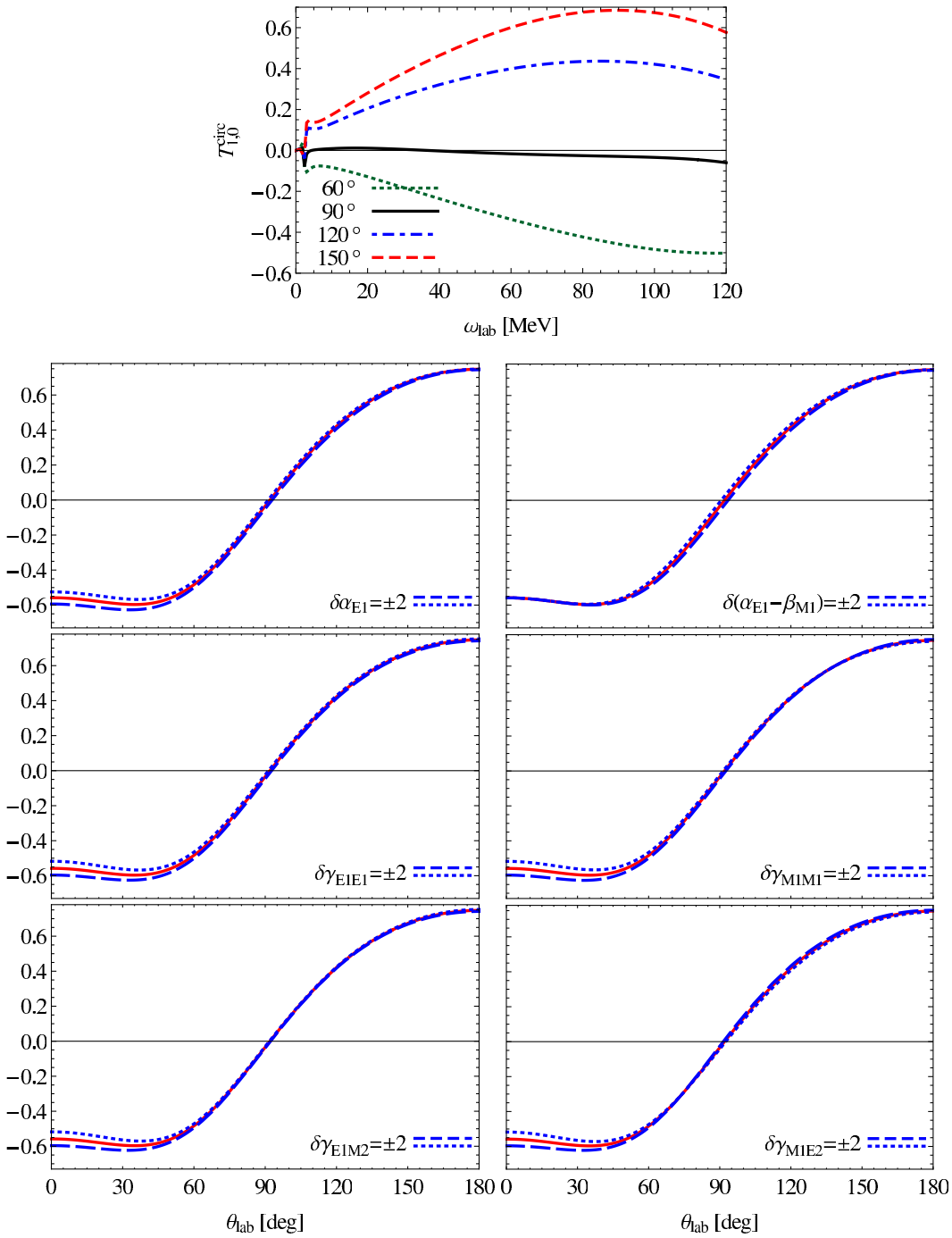

Fig. 13. (Colour on-line) Double asymmetry $T_{10}^{\rm circ}$ (lab frame). See fig. 6 for notes.

ergy, as tests with AV18 [50], Nijmegen 93 [55] and other wave functions demonstrate.

Not surprising is also that $\Delta(1232)$ effects become more pronounced with increasing energy. It is now well understood that its spin-flip amplitude considerably changes the shape of the unpolarised differential cross section at backward angles [35,36,56], thereby solving the "SAL puzzle" of deuteron Compton data at 94 MeV [12, 13, 44, 54, 57–59]. While the influence of the Delta on some observables like $\Sigma^{\rm lin}$ may be very small, it is hard to imagine an EFT without it to be reliable at photon energies around 100 MeV. As a case in point, $T_{20}^{\rm lin}$ is at 100 MeV increased by 50% and changes shape when the Delta is included; $T_{10}^{\rm circ}$ increases by 30%, while T_{21} is reduced by 20%, and $T_{22}^{\rm lin}$ even by 50%. T_{20} changes shape at forward angles. Delta effects cannot be neglected above about 70 MeV, especially in the large momentum transfers at back angles.

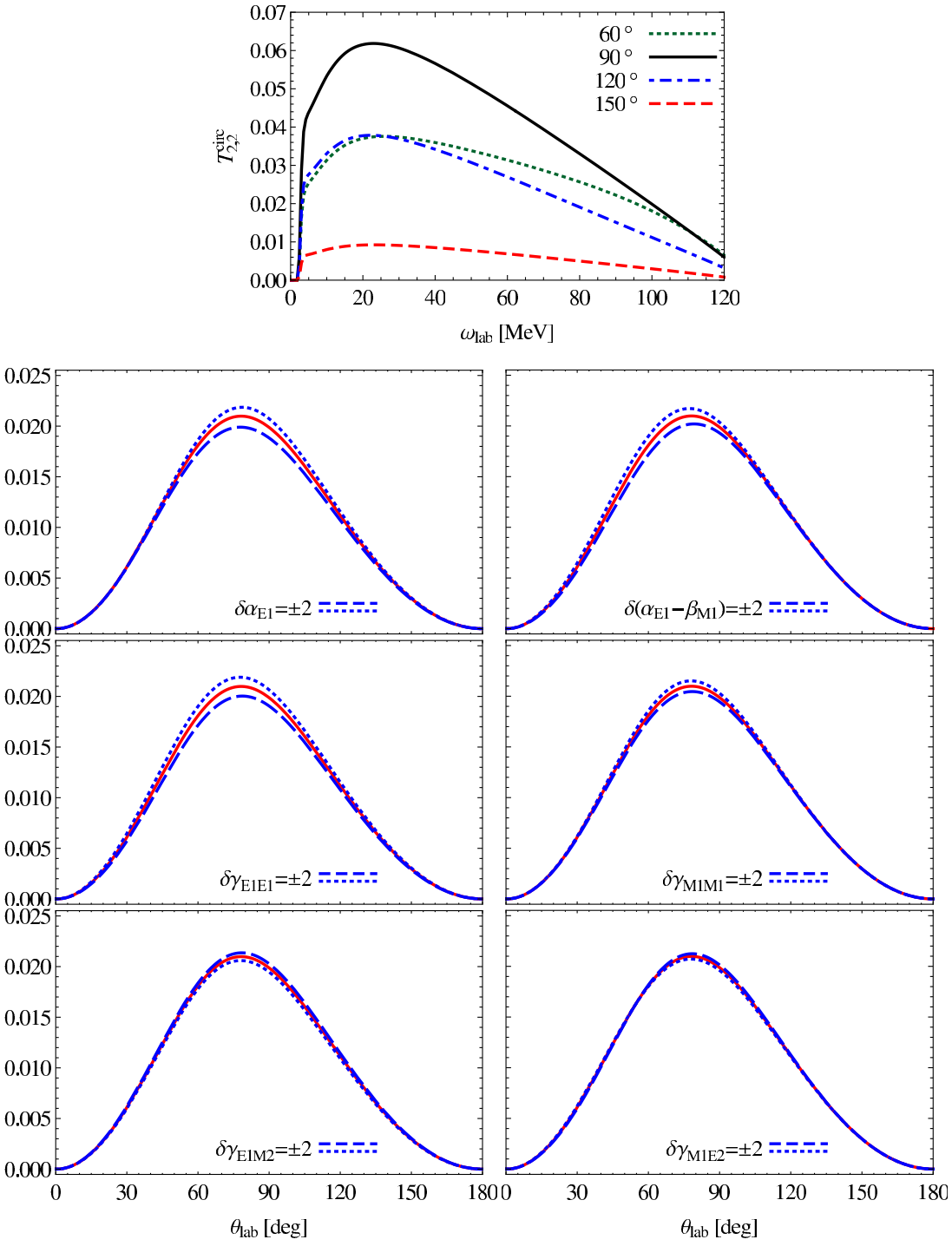

Fig. 14. (Colour on-line) Double asymmetry $T_{22}^{\rm circ}$ (lab frame). See fig. 6 for notes.

4 Conclusions and outlook

Based on a well-known decomposition of the deuteron photo-dissociation cross section, this work presented a classification of all 18 independent observables in Compton scattering off an unpolarised, vector, tensor or mixed-polarised spin-1 target with unpolarised, circularly, linearly or mixed-polarised beam when final-state polarisations are not detected. The unpolarised cross section, beam asymmetry, 4 target asymmetries and 12 double asymmetries were expressed in terms of the helicity amplitudes and related to previously used, incomplete parametrisations. This decomposition is particularly transparent, with each observable readily translated into specific and well-known beam/target/detector combinations.

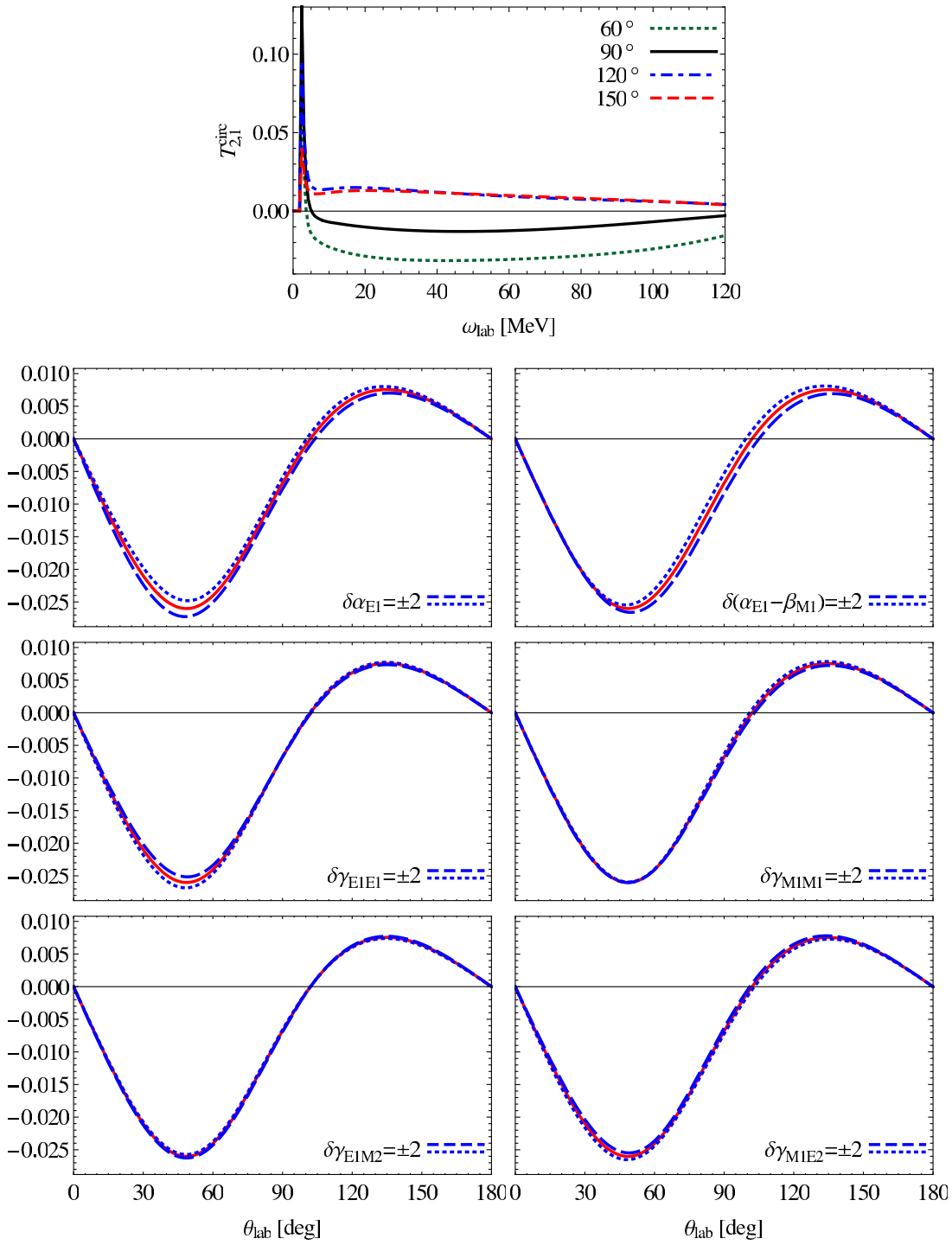

Fig. 15. (Colour on-line) Double asymmetry $T_{21}^{\rm circ}$ (lab frame). See fig. 6 for notes.

The method was then applied to deuteron Compton scattering in χEFT with dynamical $\Delta(1232)$ degrees of freedom using amplitudes which are complete at order $e^2\delta^3$ in the energy range from the Thomson limit to just below the pion production threshold. Since this process tests the isoscalar two-photon response of the nucleon, embedded in the simplest bound few-nucleon system [1], the sensitivity of each observable on the 6 dipole polarisabilities of the nucleon was studied. These, in turn, encode information on the symmetries and strengths of the interactions with and between the hadronic internal low-energy degrees of freedom. They characterise the radiation multipoles which are generated by displacing the charges and currents inside the nucleon in the electric or magnetic field of a photon with definite energy and multipolarity. To determine in particular the 4 spin polaris-

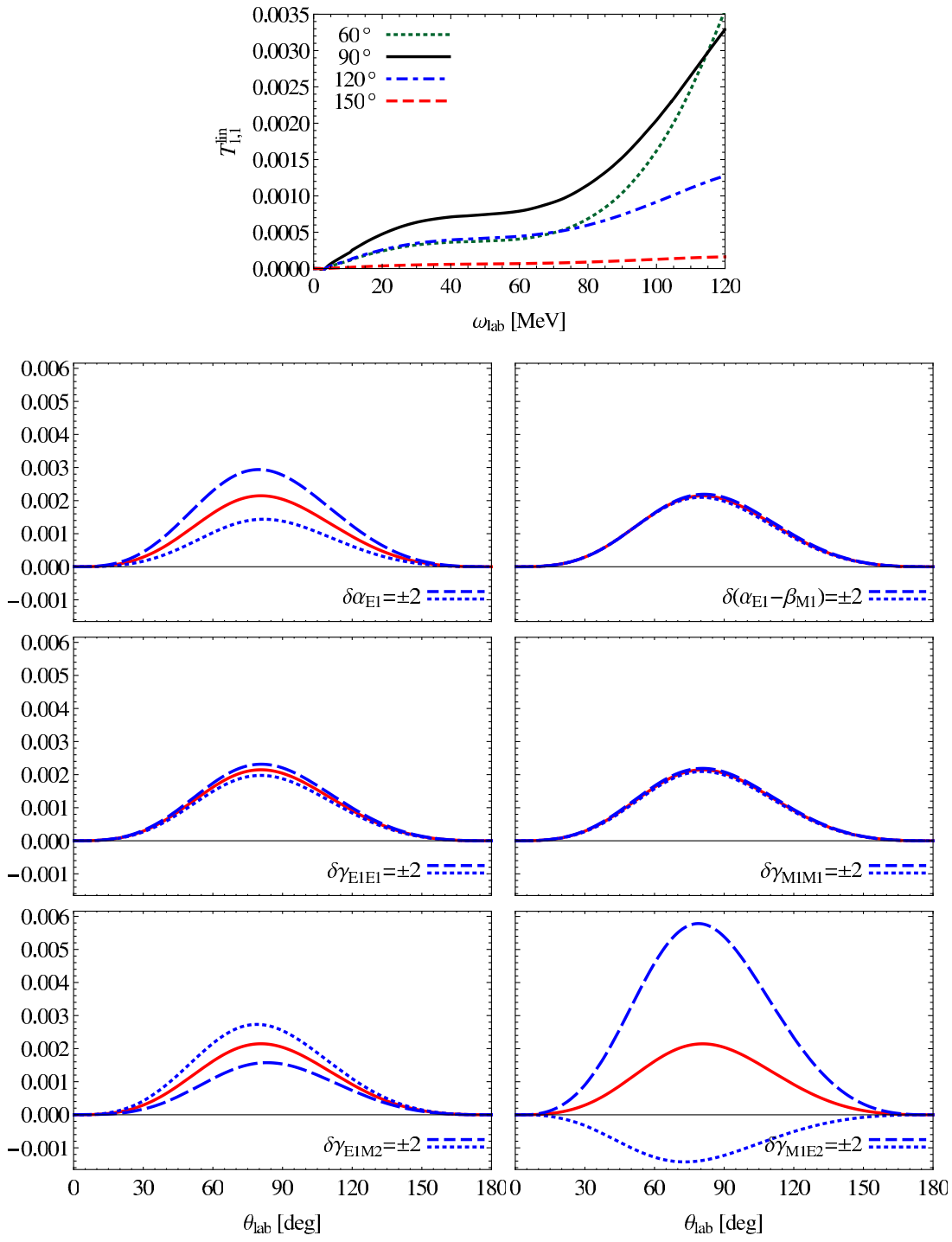

Fig. 16. (Colour on-line) Double asymmetry $T_{11}^{\rm lin}$ (lab frame). See fig. 6 for notes.

abilities is the objective of a large-scale effort including HIγS, MAX-Lab and MAMI, since they parametrise the response of the nucleon spin degrees of freedom but are not yet well-constrained. This study thus aids in planning and analysing experiments to determine the nucleon polarisabilities from deuteron Compton scattering. An interactive *Mathematica 9.0* notebook of its results over a wide range of energies is available from `hgrie@gwu.edu`.

With future high-accuracy determinations of the scalar polarisabilities α_{E1} and β_{M1} at lower energies, the spin polarisabilities seem to be reliably extractable at energies of $\gtrsim 100\,$MeV from the observables $T_{11}^{\rm circ}$ (circularly polarised beam on vector target), $T_{2(2,1)}$ (unpolarised beam on tensor target) and $T_{2(1,0)}^{\rm lin}$ (linearly polarised beam on tensor target). This experimentally challenging but realistic set consists of asymmetries which have maxima

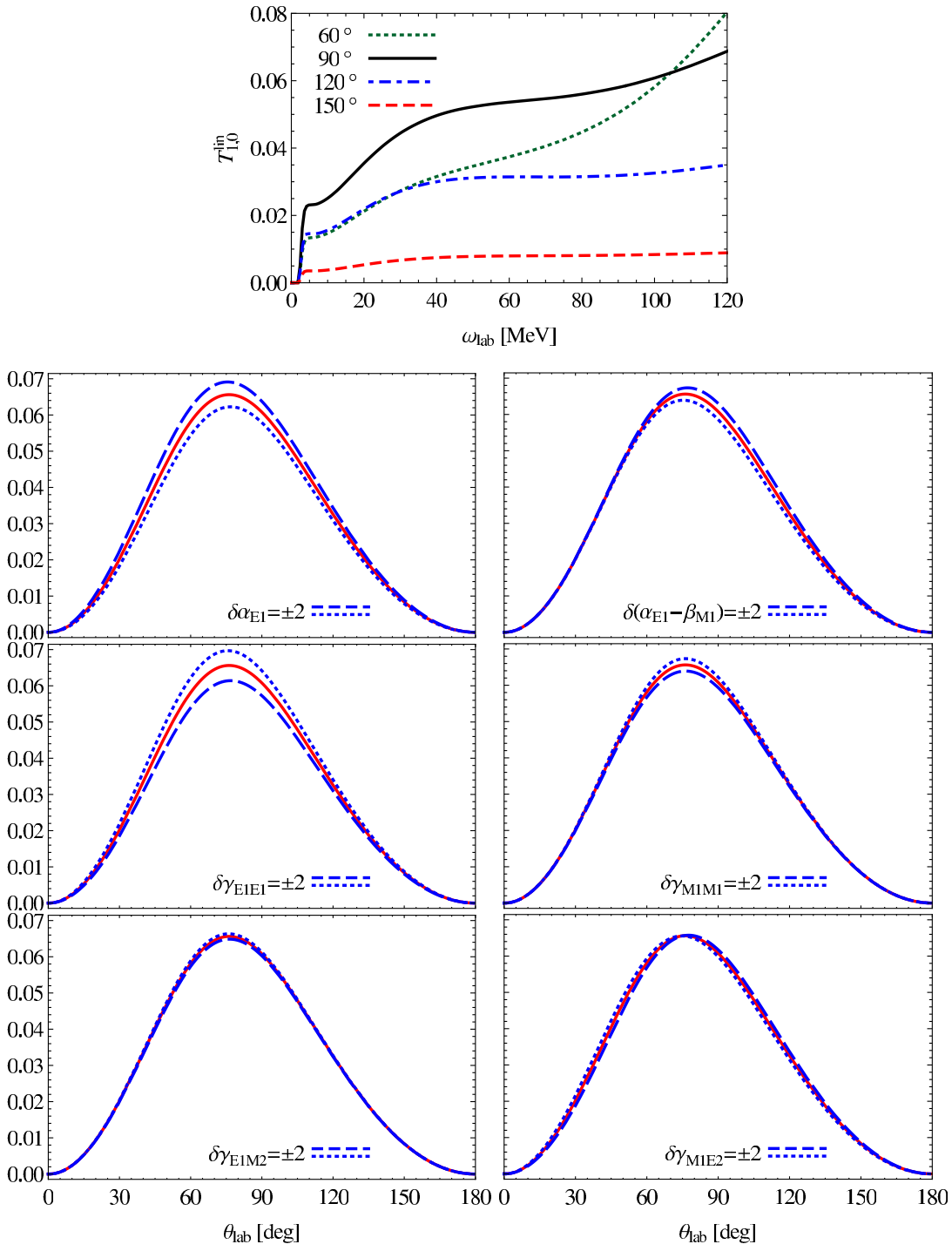

Fig. 17. (Colour on-line) Double asymmetry $T_{10}^{\rm lin}$ (lab frame). See fig. 6 for notes.

from 0.3 to 0.05 and are mostly sensitive to only 1 or 2 polarisabilities. Modifying the spin polarisabilities by $\pm 2\times 10^{-4}\,\mathrm{fm}^4$ in them induces variations of ±5% to ±20% at 100 MeV.

Since nuclear binding is mediated by charged pion-exchange currents to which the photons can couple, deuteron Compton scattering concurrently tests the detailed symmetries and dynamics of the charged part of the two-nucleon interaction. The D wave contributions of the deuteron wave function and of the pion-exchange currents lead to nonzero tensor observables. By interference with the quadrupole components of the incident and outgoing photon, these, in turn, seem to be much more sensitive on the mixed spin polarisabilities γ_{E1M2} and γ_{M1E2} than any single-nucleon observable. One may thus speculate that their determination will first appear from deuteron data —if the necessary accuracy can be reached.

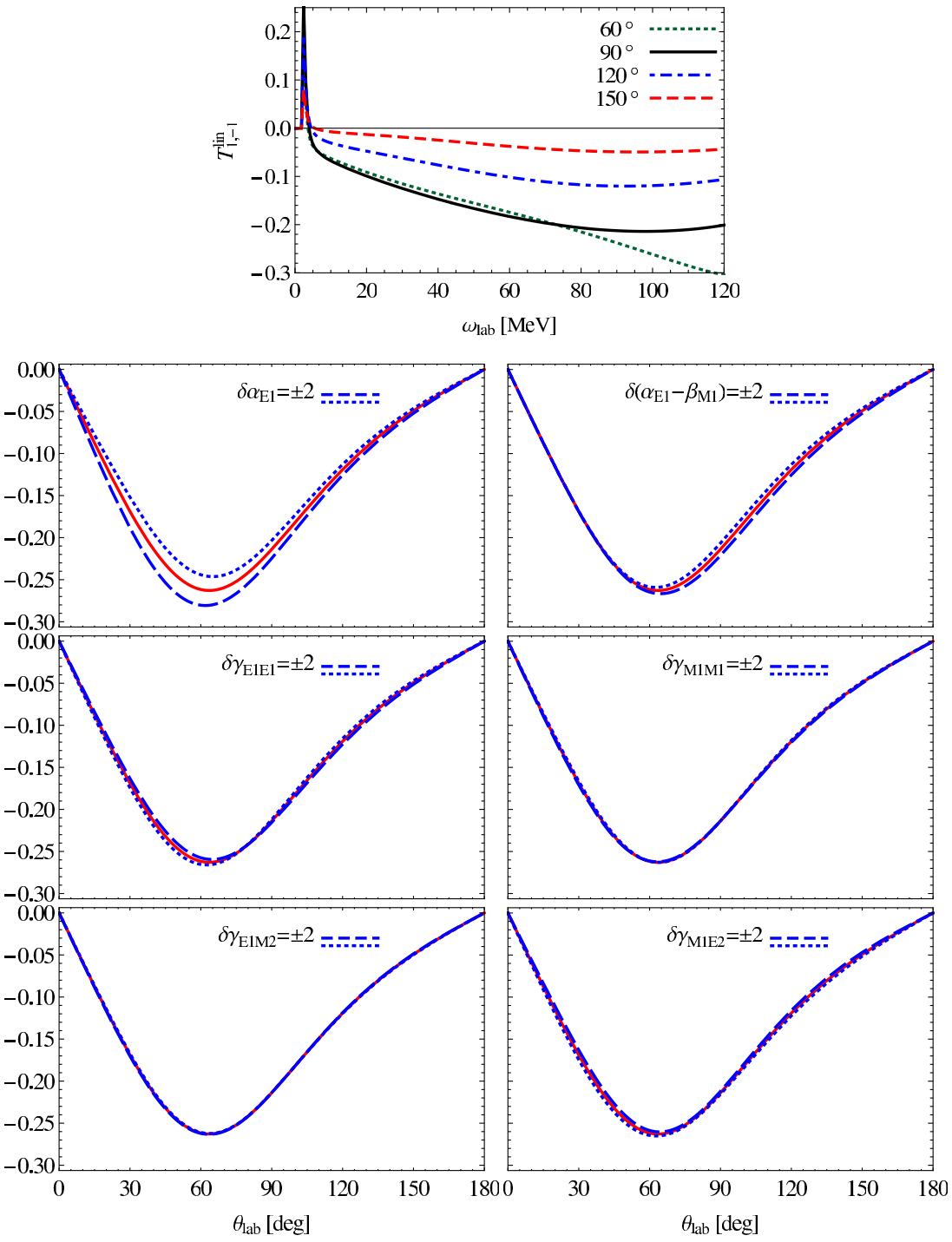

Fig. 18. (Colour on-line) Double asymmetry $T^{\rm lin}_{1,-1}$ (lab frame). See fig. 6 for notes.

Ongoing work includes embedding the $\mathcal{O}(e^2\delta^4)$ single-nucleon amplitudes of ref. [29] for an extension to photon energies above the pion-production threshold, also with Δ-ful pion-exchange currents; inclusion of a chirally consistent NN potential; and a detailed assessment of theoretical uncertainties. In support of ongoing and planned experiments at HIγS, MAX-Lab and MAMI, this effort is pursued in the context of a comprehensive theoretical description of Compton scattering on the proton, deuteron and ^{3}He in χEFT, valid from zero photon energy well into the Δ resonance region. As pendant to the present article, a classification of the independent polarisation transfer observables on a spin-1 target will determine those 5 which are linearly independent and complement those presented here for the complete set of 23 independent observables [15]. From these, the 23 independent real amplitudes

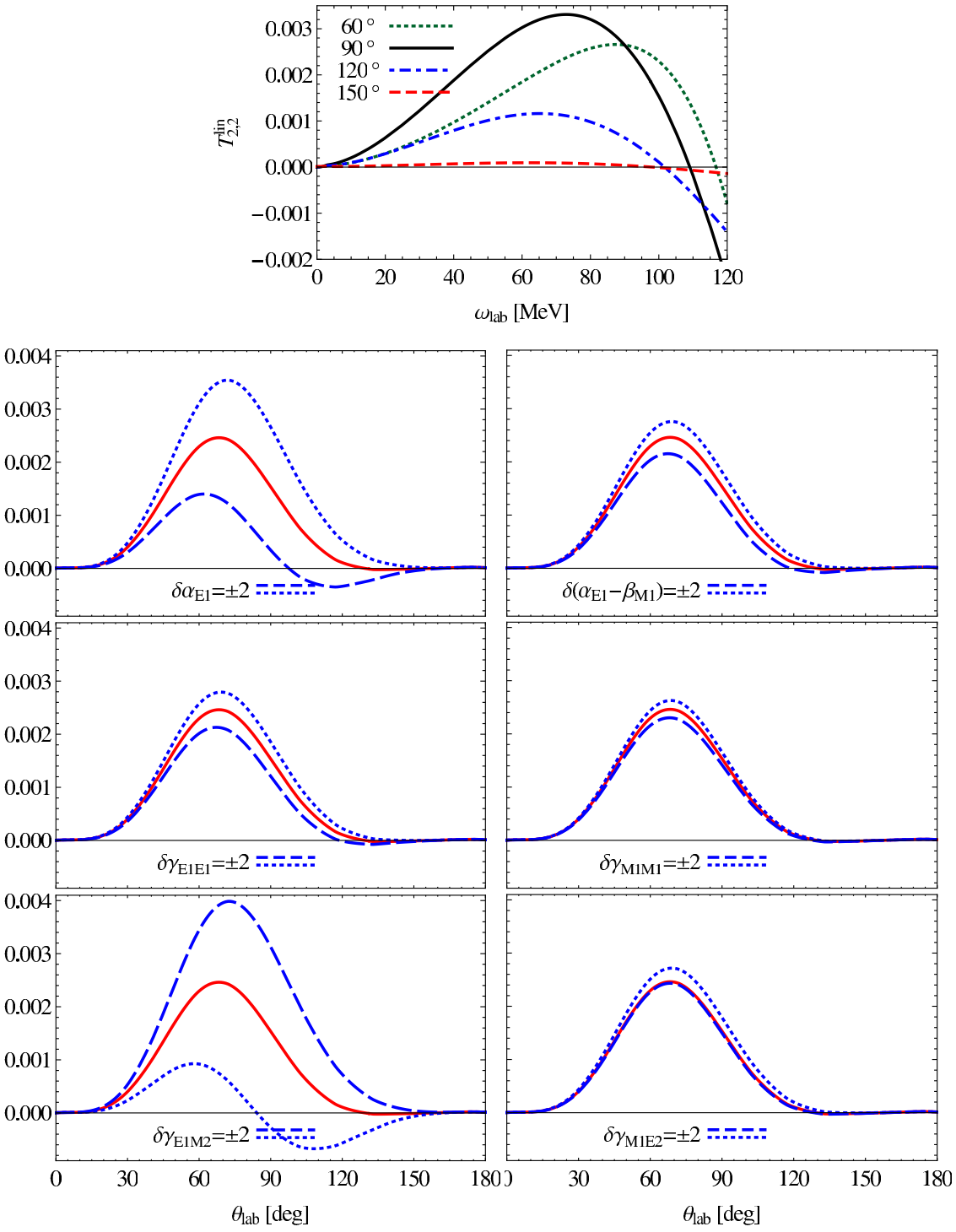

Fig. 19. (Colour on-line) Double asymmetry $T_{22}^{\rm lin}$ (lab frame). See fig. 6 for notes.

can be reconstructed in turn, and hence all information accessible in the two-photon response of the deuteron and its constituents.

Finally, I offer to embed single-nucleon Compton amplitudes, chiral or not, into the available deuteron code, so that other theoretical descriptions can be tested collaboratively.

I am particularly indebted to my Compton collaborators, J.A. McGovern and D.R. Phillips, for discussions and encouragement, and to the organisers and participants of the INT workshop 12-3: "Light Nuclei from First Principles" as well as the "Workshop to Explore Physics Opportunities with Intense, Polarized Electron Beams with Energy up to 300 MeV" at the MIT, both of which also provided finan-

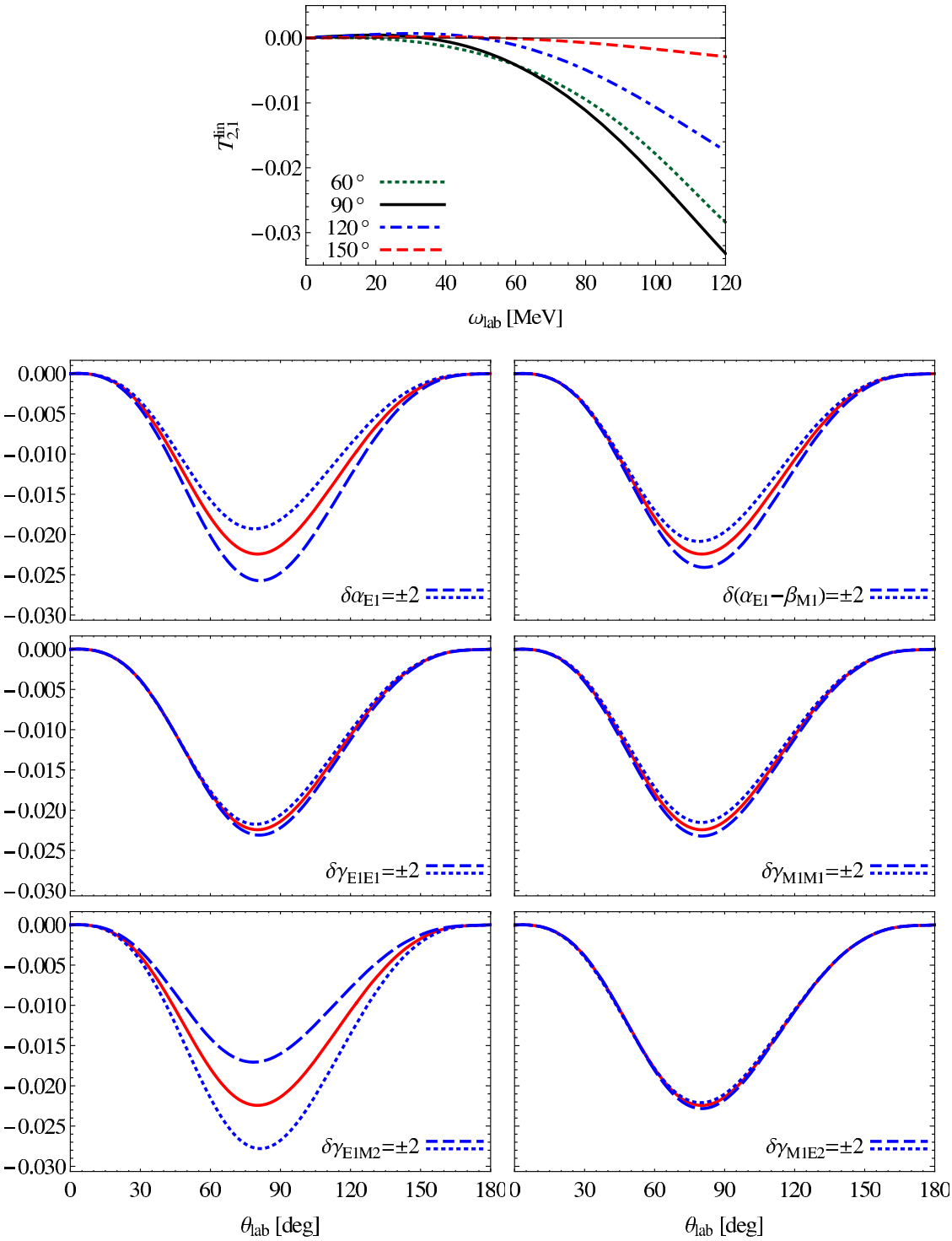

Fig. 20. (Colour on-line) Double asymmetry $T_{21}^{\rm lin}$ (lab frame). See fig. 6 for notes.

cial support. D.G. Crabb and W. Meyer shared their expertise on tensor-polarised targets, and R. Schiavilla the crucial hint to ref. [14]. Discussions with W. Briscoe, E. Downie, G. Feldman and H. Weller helped clarify various experimental points. This work was supported in part by the National Science Foundation under CAREER award PHY-0645498, by the US-Department of Energy under contract DE-FG02-95ER-40907, by the Deutsche Forschungsgemeinschaft and the National Natural Science Foundation of China through funds provided to the Sino-German CRC 110 "Symmetries and the Emergence of Structure in QCD", and by the EPOS network of the European Community Research Infrastructure Integrating Activity "Study of Strongly Interacting Matter" (HadronPhysics3).

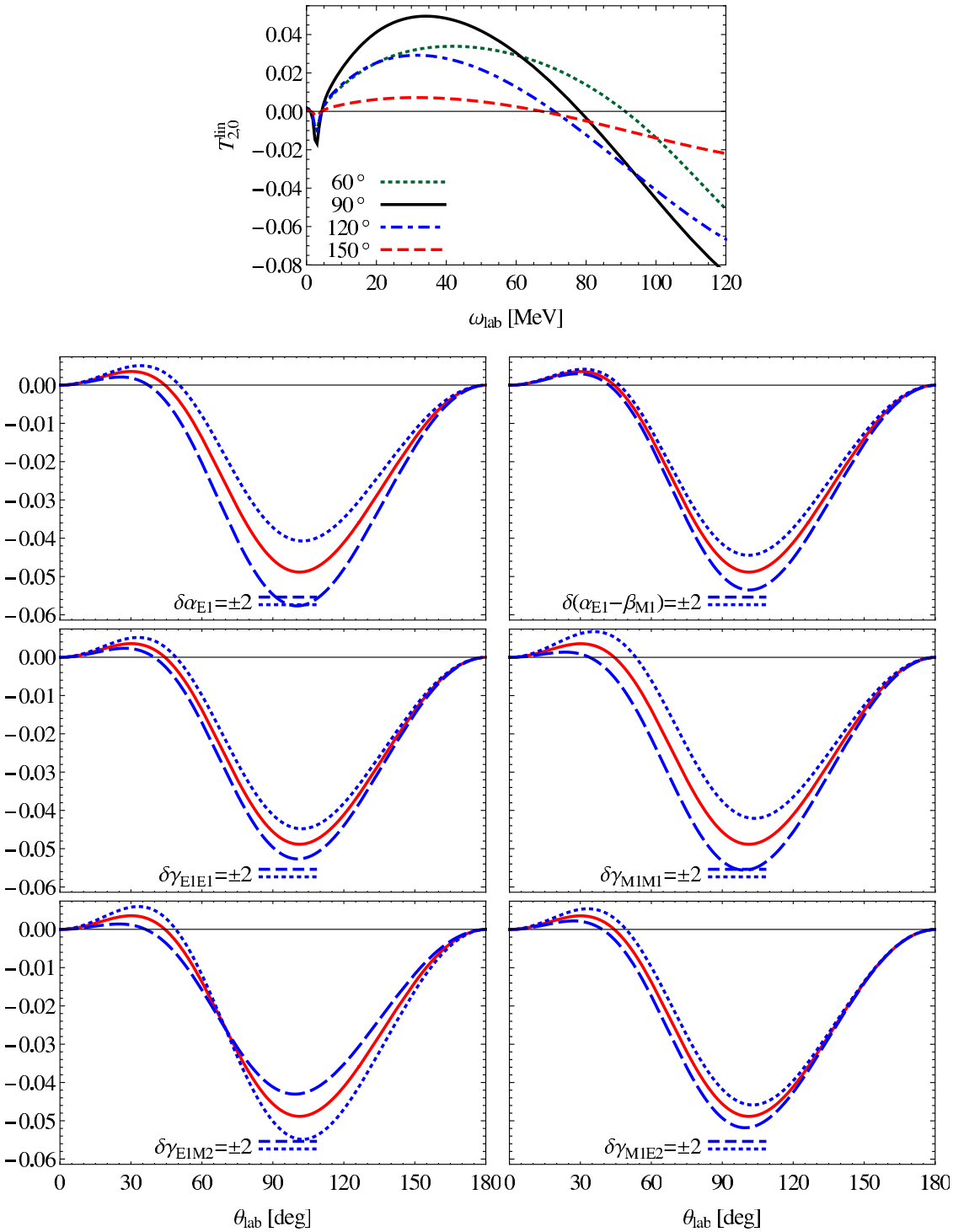

Fig. 21. (Colour on-line) Double asymmetry $T_{20}^{\rm lin}$ (lab frame). See fig. 6 for notes.

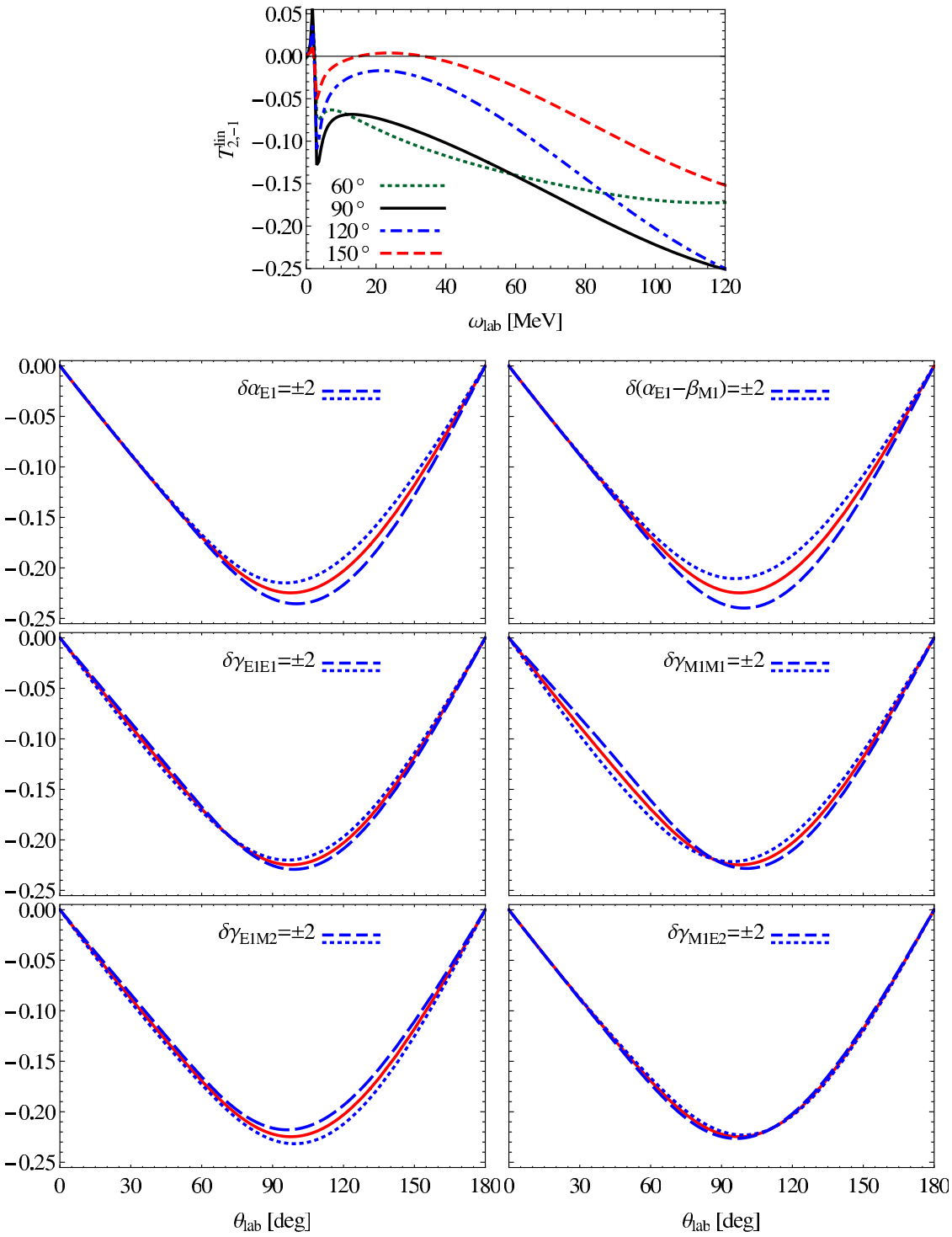

Fig. 22. (Colour on-line) Double asymmetry $T^{\rm lin}_{2,-1}$ (lab frame). See fig. 6 for notes.

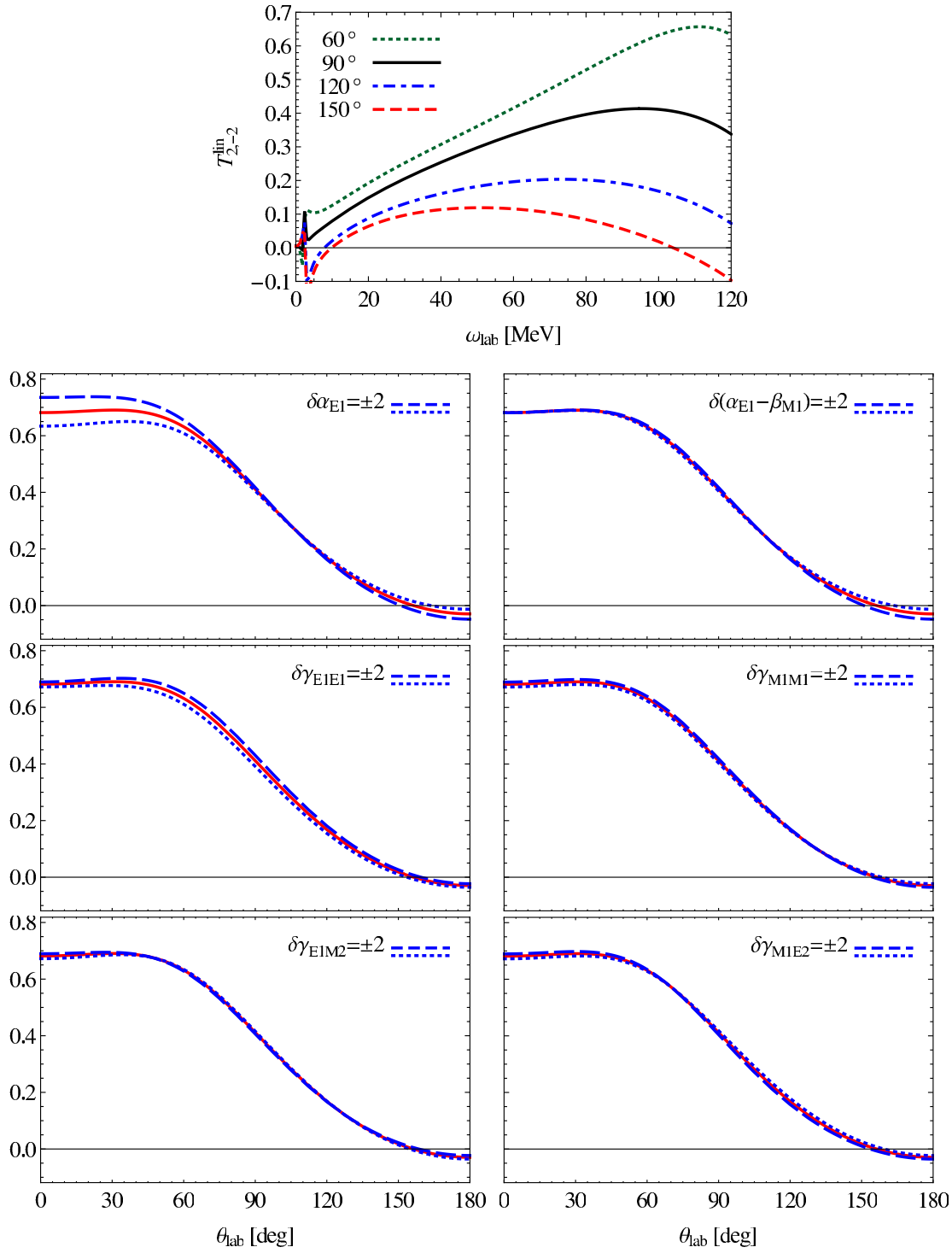

Fig. 23. (Colour on-line) Double asymmetry $T^{\rm lin}_{2,-2}$ (lab frame). See fig. 6 for notes.

References

1. H.W. Griesshammer, J.A. McGovern, D.R. Phillips, G. Feldman, Prog. Part. Nucl. Phys. **67**, 841 (2012) arXiv:1203.6834 [nucl-th].
2. H. Paetz gen. Schieck, *Nuclear Physics with Polarized Particles*, in *Lecture Notes in Physics*, Vol. **842** (Springer, 2012).
3. D.G. Crabb, private communication.
4. W. Meyer, private communication.
5. D. Babusci, G. Giordano, A.I. L'vov, G. Matone, A.M. Nathan, Phys. Rev. C **58**, 1013 (1998) arXiv:hep-ph/9803347.
6. J.W. Chen, X.d. Ji, Y.c. Li, Phys. Rev. C **71**, 044321 (2005) arXiv:nucl-th/0408004.
7. J.-W. Chen, X.-d. Ji, Y.-c. Li, Phys. Lett. B **620**, 33 (2005) arXiv:nucl-th/0408003.
8. D. Choudhury, D.R. Phillips, Phys. Rev. C **71**, 044002 (2005) arXiv:nucl-th/0411001.
9. D. Choudhury, PhD Thesis Ohio University (2006).
10. H.W. Grießhammer, D. Shukla, Eur. Phys. J. A **46**, 249 (2010) **48**, 76(E) (2012) arXiv:1006.4849 [nucl-th].
11. J.W. Chen, Nucl. Phys. A **653**, 375 (1999) arXiv:nucl-th/9810021.
12. J. Karakowski, arXiv:nucl-th/9901011.
13. J.J. Karakowski, G.A. Miller, Phys. Rev. C **60**, 014001 (1999) arXiv:nucl-th/9901018.
14. H. Arenhovel, M. Sanzone, Few-Body Syst. Suppl. **3**, 1 (1991).
15. H.W. Grießhammer, in preparation.
16. H.W. Grießhammer, T.R. Hemmert, Phys. Rev. C **65**, 045207 (2002) arXiv:nucl-th/0110006.
17. R.P. Hildebrandt, H.W. Grießhammer, T.R. Hemmert, B. Pasquini, Eur. Phys. J. A **20**, 293 (2004) arXiv:nucl-th/0307070.
18. B.R. Holstein, arXiv:hep-ph/0010129.
19. W. Detmold, B.C. Tiburzi, A. Walker-Loud, Phys. Rev. D **81**, 054502 (2010) arXiv:1001.1131 [hep-lat].
20. M. Engelhardt, PoS LATTICE **2011**, 153 (2011) arXiv:1111.3686 [hep-lat].
21. M. Lujan, A. Alexandru, F. Lee, PoS LATTICE **2011**, 165 (2011). arXiv:1111.6288 [hep-lat].
22. A. Walker-Loud, C.E. Carlson, G.A. Miller, Phys. Rev. Lett. **108**, 232301 (2012) arXiv:1203.0254 [nucl-th].
23. K. Pachucki, Phys. Rev. A **60**, 3593 (1999).
24. C.E. Carlson, M. Vanderhaeghen, arXiv:1109.3779 [physics.atom-ph].
25. M.C. Birse, J.A. McGovern, Eur. Phys. J. A **48**, 120 (2012) arXiv:1206.3030 [hep-ph].
26. G.A. Miller, Phys. Lett. B **718**, 1078 (2013) arXiv:1209.4667 [nucl-th].
27. V. Bernard, N. Kaiser, U.G. Meißner, Phys. Rev. Lett. **67**, 1515 (1991).
28. V. Bernard, N. Kaiser, U.G. Meißner, Int. J. Mod. Phys. E **4**, 193 (1995) arXiv:hep-ph/9501384.
29. J.A. McGovern, D.R. Phillips, H.W. Grießhammer, Eur. Phys. J. A **49**, 12 (2013) arXiv:1210.4104 [nucl-th].
30. M. Schumacher, Prog. Part. Nucl. Phys. **55**, 567 (2005) arXiv:hep-ph/0501167.
31. H.W. Grießhammer, D.R. Phillips, J.A. McGovern, arXiv:1306.2200 [nucl-th].
32. M.E. Rose, *Elementary Theory of Angular Momentum* (Wiley, 1957).
33. A.R. Edmonds, *Angular Momentum in Quantum Mechanics* (Princeton University Press, 1974).
34. Particle Data Group, Phys. Rev. D **86**, 010001 (2012).
35. R.P. Hildebrandt, H.W. Grießhammer, T.R. Hemmert, Eur. Phys. J. A **46**, 111 (2010) arXiv:nucl-th/0512063.
36. R.P. Hildebrandt, *Elastic Compton Scattering from the Nucleon and Deuteron*, PhD Thesis Technische Universität München (2005) arXiv:nucl-th/0512064.
37. V. Pascalutsa, D.R. Phillips, Phys. Rev. C **67**, 055202 (2003) arXiv:nucl-th/0212024.
38. H.W. Grießhammer, Proceedings Menu 2007, eConf section of the SLAC archive, arXiv:0710.2924.
39. H.W. Grießhammer, Prog. Part. Nucl. Phys. **55**, 215 (2005) arXiv:nucl-th/0411080.
40. E.E. Jenkins, A.V. Manohar, Phys. Lett. B **255**, 558 (1991).
41. E.E. Jenkins, A.V. Manohar, In *Dobogokoe 1991, Proceedings, Effective field theories of the standard model* 113 and Calif. Univ. San Diego - UCSD-PTH 91-30 (91/10, rec. Dec.) (201392) p. 26 (see conference index).
42. T.R. Hemmert, B.R. Holstein, J. Kambor, Phys. Lett. B **395**, 89 (1997) arXiv:hep-ph/9606456.
43. T.R. Hemmert, B.R. Holstein, J. Kambor, J. Phys. G **24**, 1831 (1998) arXiv:hep-ph/9712496.
44. S.R. Beane, M. Malheiro, D.R. Phillips, U. van Kolck, Nucl. Phys. A **656**, 367 (1999) arXiv:nucl-th/9905023.
45. J.L. Friar, Ann. Phys. (NY) **95**, 170 (1975).
46. J.L. Friar, Phys. Rev. C **16**, 1504 (1977).
47. H. Arenhovel, Z. Phys. A **297**, 129 (1980).
48. M. Weyrauch, H. Arenhovel, Nucl. Phys. A **408**, 425 (1983).
49. E. Epelbaum, W. Gloeckle, U.-G. Meißner, Nucl. Phys. A **671**, 295 (2000) arXiv:nucl-th/9910064.
50. R.B. Wiringa, V.G.J. Stoks, R. Schiavilla, Phys. Rev. C **51**, 38 (1995).
51. R. Miskimen, *Measuring the Spin-Polarizabilities of the Proton at HIγS* , presentation at the INT workshop on Soft Photons and Light Nuclei, 17 June 2008, and private communication.
52. K. Aulenbacher, talk given at the *Workshop to Explore Physics Opportunities with Intense, Polarized Electron Beams with Energy up to* 300 MeV, MIT, 2013, in preparation.
53. L.C. Maximon, Phys. Rev. C **39**, 347 (1989).
54. S.R. Beane, M. Malheiro, J.A. McGovern, D.R. Phillips, U. van Kolck, Nucl. Phys. A **747**, 311 (2005) arXiv:nucl-th/0403088.
55. V.G. Stoks, R.A. Klomp, C.P. Terheggen, J.J. de Swart, Phys. Rev. C **49**, 2950 (1994).
56. R.P. Hildebrandt, H.W. Grießhammer, T.R. Hemmert, D.R. Phillips, Nucl. Phys. A **748**, 573 (2005) arXiv:nucl-th/0405077.
57. S.R. Beane, M. Malheiro, J.A. McGovern, D.R. Phillips, U. van Kolck, Phys. Lett. B **567**, 200 (2003) arXiv:nucl-th/0209002.
58. D.L. Hornidge, B.J. Warkentin, R. Igarashi, J.C. Bergstrom, E.L. Hallin, N.R. Kolb, R.E. Pywell, D.M. Skopik *et al.*, Phys. Rev. Lett. **84**, 2334 (2000) arXiv:nucl-ex/9909015.
59. M.I. Levchuk, A.I. L'vov, Nucl. Phys. A **674**, 449 (2000) arXiv:nucl-th/9909066.